

Periglacial landscape evolution and environmental changes of Arctic lowland areas for the last 60 000 years (western Laptev Sea coast, Cape Mamontov Klyk)

Lutz Schirrmeister¹, Guido Grosse², Viktor Kunitsky³, Diana Magens¹, Hanno Meyer¹, Alexander Dereviagin⁴, Tatyana Kuznetsova⁴, Andrei Andreev¹, Olga Babiy³, Frank Kienast⁵, Mikhael Grigoriev³, Pier Paul Overduin¹ & Frank Preusser⁶

- 1 Alfred Wegener Institute for Polar and Marine Research, Telegrafenberg A43, DE-14473 Potsdam, Germany
- 2 Geophysical Institute, University of Alaska Fairbanks, 903 Koyukuk Drive, Fairbanks, AK 99775, USA
- 3 Permafrost Institute, Siberian Branch Russian Academy of Science, RU-677010 Yakutsk, Russia
- 4 Faculty of Geology, Moscow State University, Vorobievsky Gory, RU-119992 Moscow, Russia
- 5 Senckenberg Institute for Quaternary Palaeontology, Am Jakobskirchhof 4, DE-99423 Weimar, Germany
- 6 University Bern, Institute of Geology, Baltzerstrasse 1-3, CH-3012 Bern, Switzerland

Keywords

Late Quaternary; north-east Siberia; palaeoenvironment; permafrost.

Correspondence

L. Schirrmeister, Alfred Wegener Institute for Polar and Marine Research, Telegrafenberg A43, DE-14473 Potsdam, Germany. E-mail: Lutz.Schirrmeister@awi.de

doi:10.1111/j.1751-8369.2008.00067.x

Abstract

Non-glaciated Arctic lowlands in north-east Siberia were subjected to extensive landscape and environmental changes during the Late Quaternary. Coastal cliffs along the Arctic shelf seas expose terrestrial archives containing numerous palaeoenvironmental indicators (e.g., pollen, plant macro-fossils and mammal fossils) preserved in the permafrost. The presented sedimentological (grain size, magnetic susceptibility and biogeochemical parameters), cryolithological, geochronological (radiocarbon, accelerator mass spectrometry and infrared-stimulated luminescence), heavy mineral and palaeoecological records from Cape Mamontov Klyk record the environmental dynamics of an Arctic shelf lowland east of the Taymyr Peninsula, and thus, near the eastern edge of the Eurasian ice sheet, over the last 60 Ky. This region is also considered to be the westernmost part of Beringia, the non-glaciated landmass that lay between the Eurasian and the Laurentian ice caps during the Late Pleistocene. Several units and subunits of sand deposits, peat–sand alternations, ice-rich palaeocrysol sequences (Ice Complex) and peaty fillings of thermokarst depressions and valleys were presented. The recorded proxy data sets reflect cold stadial climate conditions between 60 and 50 Kya, moderate interstadial conditions between 50 and 25 Kya and cold stadial conditions from 25 to 15 Kya. The Late Pleistocene to Holocene transition, including the Allerød warm period, the early to middle Holocene thermal optimum and the late Holocene cooling, are also recorded. Three phases of landscape dynamic (fluvial/alluvial, irregular slope run-off and thermokarst) were presented in a schematic model, and were subsequently correlated with the supraregional environmental history between the Early Weichselian and the Holocene.

Permafrost is the most widely distributed, climatically induced geophysical phenomenon in terrestrial polar regions. Extreme cooling under the influence of stable eastern Siberian anticyclone winter conditions was a prerequisite for the formation of thick and spatially extensive permafrost. The permafrost in eastern Siberia is closely connected with cold and dry climate conditions, stable over long periods, and the absence of large ice sheets in

the past. During the Late Pleistocene cold periods, global sea level lowering exposed large portions of the Arctic shelves, and an extensive subaerial shelf plain was formed in north-eastern Siberia. Various palaeoenvironmental records are preserved in permafrost sequences that are exposed along Siberian Arctic coasts and riverbanks. They were used for reconstructing the Late Pleistocene–Holocene palaeoenvironment of the

Laptev Sea region, which has been intensively studied during the last 10 years by joint projects within the framework of the Russian–German scientific collaboration “System Laptev Sea”. Both frozen sediment sequences and ground ice are considered archives rich in palaeoenvironmental information. For their investigation, a multidisciplinary approach was used in order to understand different aspects of Arctic environmental conditions and their variations during the Late Quaternary. Records were studied with various disciplines, such as geocryology, sedimentology, pedology, geomorphology, hydrochemistry, isotope geochemistry of ground ice and palaeoecology (e.g., Schirrmeister, Siegert, Kunitsky et al. 2002; Schirrmeister, Siegert, Kuznetsova et al. 2002; Meyer, Dereviagin, Siegert & Hubberten 2002; Meyer, Dereviagin, Siegert, Schirrmeister & Hubberten 2002; Andreev et al. 2002; Kienast et al. 2005; Kienast et al. 2008). Fieldwork at Cape Mamontov Klyk in the western Laptev Sea region of Arctic Siberia in the summer of 2003 (Fig. 1) followed this approach (Schirrmeister et al. 2004). Permafrost archives are the only available long-term palaeoenvironmental records in north-east Siberia. Exposures such as the one presented here offer transects across buried Late Quaternary landscapes, and thus reflect the spatial variability of the landscape and the genetic processes leading to its development.

This paper represents the first compilation of numerous local palaeoenvironmental data from the western Laptev Sea region. The objective is to interpret palaeo-climate, landscape and permafrost dynamics of the region during the last 50 Ky, and to integrate these with knowledge about the Late Quaternary environmental history of the Eurasian north. The presented palaeoenvironmental records serve as reference datasets for ongoing studies of offshore subsea permafrost deposits at the Cape Mamontov Klyk coast (Rachold et al. 2007).

Geography and geology of the study site

Mamontov Klyk lies within the continuous permafrost zone, with permafrost reaching 200–300 m in depth (Williams & Warren 1999). The regional geomorphology is determined by the Pronchishchev Ridge in the south, stretching parallel to the coast from north-west to south-east, and a 30–40-km-wide sedimentary plain north of these mountains (Fig. 1a). The maximum height of the Pronchishchev Ridge (315 m a.s.l.) is reached in the headwaters of the Urasalakh River. The sedimentary plain is gently inclined towards the Laptev Sea coast with heights from 60 to 75 m a.s.l. close to the Pronchishchev Ridge, and 25–35 m a.s.l. at the coast (with an inclination angle of $<0.1^\circ$). Watersheds are characterized by large streams that originate in the southern hill range and flow

through wide valleys with gentle slopes, and by dendritic nets of thermoerosional valleys with steep slopes and flat bottoms, which drain the higher elevations of the lowland plain (Fig. 1b; Grosse et al. 2006). The major river flow directions in the region are either south–north or west–east. Some of the large rivers cross the south-eastern Pronchishchev Ridge on their way northwards, which can only be explained by recent neotectonic uplift of the Pronchishchev Ridge.

Thermokarst depressions are widely distributed on the sedimentary plain. They occur not only along river valleys but also on interfluvies between the river valleys. Most of the elliptical thermokarst basins are oriented in a north–south direction (Fig. 1b). Remote sensing analyses indicate that about 78% of the plain is affected to some degree by permafrost degradation (Grosse et al. 2006). The study area in the vicinity of Cape Mamontov Klyk is situated near the mouth of the Nuchcha Dzhihle River, a meandering stream several tens of metres wide. The study area consists of Yedoma hills (20–40 m a.s.l.), which are separated by several thermoerosional valleys, and thermokarst depressions. Yedoma hills consist of ice-rich permafrost sequences with wide and deep ice wedges, and are erosional remnants of a former periglacial accumulation plain. Yedoma is a special relief form resulting from thermokarst processes affecting ice-rich permafrost landscapes in Yakutia (Solov'ev 1959, 1989). We consider Yedoma to be a morphological structure that is composed of a suite of ice-rich permafrost deposits: the “Ice Complex” (Schirrmeister et al. 2008). The term “Ice Complex” (*Ledovji Kompleks* in Russian) was introduced by Solov'ev in 1959. The investigated profiles are located in ice-rich sediments exposed on the coastal bluff, which reaches heights between 10 and 25 m a.s.l. (Figs. 2 and 3).

The Quaternary geological history of the coastal lowland at the Lena–Anabar interfluvium remains poorly understood. Russian geologists such as Toll (1894), Čekanovskiy (1896) and Tolmačev (1905) made the first geological observations of the region. Toll (1894) provided initial information on the environment, geology and relict ground ice. In an early interpretation, Toll (1894) assumed the huge relict ice bodies observed along the coast to be the remnants of buried glacial ice. New and often contradictory information on the Quaternary geology of the coastal lowland was collected during geological surveys conducted in the second half of the 20th century. Ice-rich silty sand deposits exposed at the lowland coast were interpreted as marine sediments (Sočava 1933; Žukov et al. 1968), fluvio-glacial and fluvial-lacustrine deposits (Puminov 1962), cryogenic-aolian or fluvial-lacustrine deposits (Kolpakov 1973). These investigations are usually based on the well-known stratigraphical scheme of Saks (1953) for the Russian

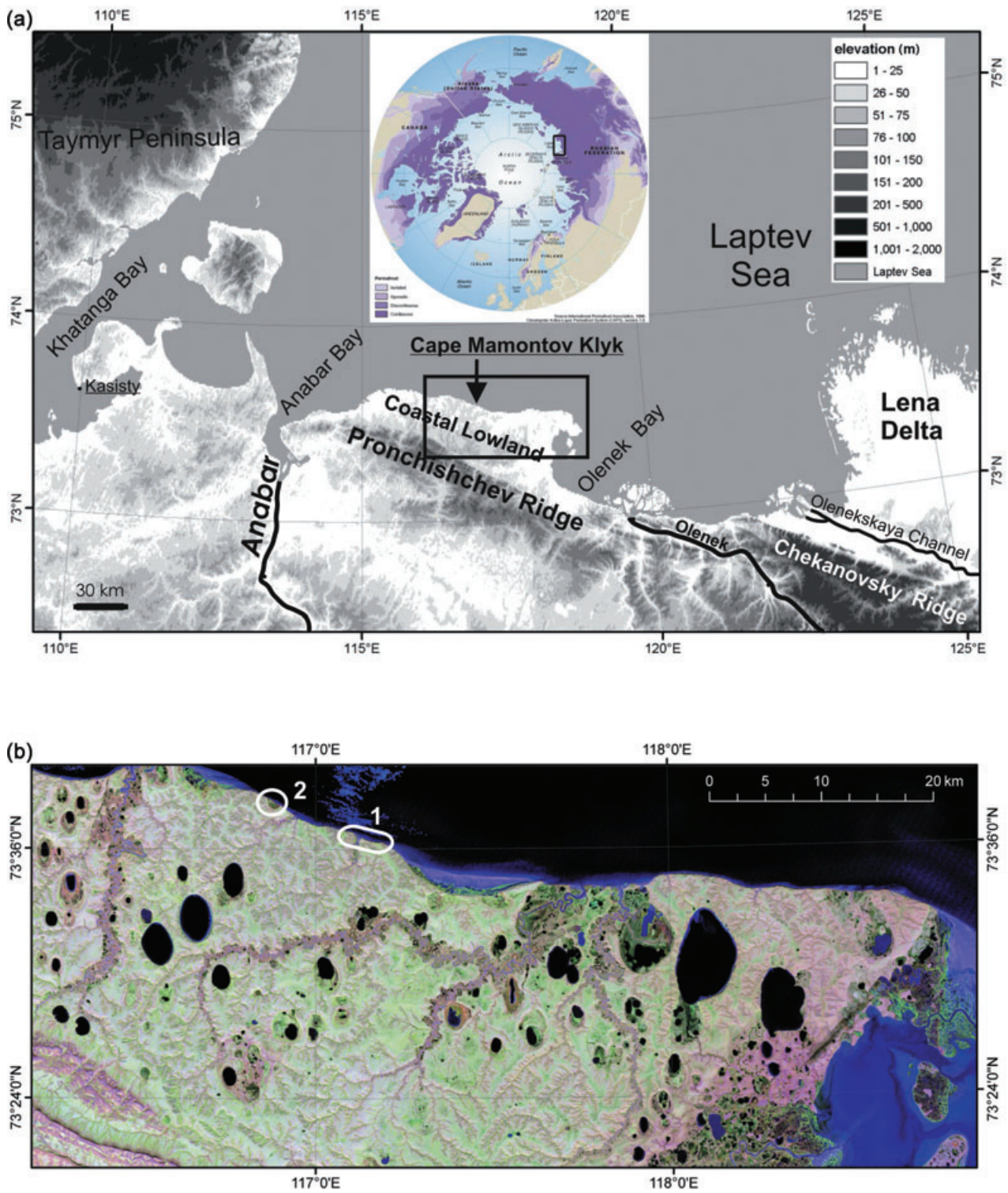


Fig. 1 Study area. (a) Position of the study area on the coast of the Olenek–Anabar interfluve in the western Laptev Sea. The black arrow marks the position of the coastal exposure of Cape Mamontov Klyk. The small inset map shows the distribution of permafrost types (UNEP/GRID-Arendal 2005) and the location of the study area in the Arctic. (b) Landsat-7 satellite image of the thermokarst-affected coastal lowland in front of the Pronchishchev Ridge. Study sites: 1, main study section around Cape Mamontov Klyk; 2, additional study site with thermokarst lake deposits.

north. Bojarskij & Mitt (1961) correctly defined ice bodies in the ice-rich sediments of the coastal outcrops as large syngenetic ice wedges.

The study area is located in the north-eastern part of the Lena–Anabar depression, in the Olenek zone of the Late Mesozoic folded complex, at the boundary of the Siberian Craton and the Laptev Paraplatformal Block (Drachev et al. 1998). The main structural elements of the territory are the Upper Cretaceous to Cenozoic onshore sedimentary cover (terrestrial and shelf parts) and the Lena–Taymyr uplift (the recent shelf part). The entire Laptev Sea region was, and continues to be, seismically active up until the present day.

Material and methods

The coastal bluff was divided into several subsections. Surveying of vertical profile lines, the coastline and outcrop areas were carried out using a laser tachymeter (Zeiss ELTA 3) and measuring tape, followed by an initial stratigraphic assessment and detailed sampling of the permafrost sequences. In general, field studies were difficult because of the limited accessibility of the steep permafrost outcrops and extensive mudflows on the slopes. Two large vertical composite profiles (profiles 1 and 2) were obtained consisting of several subprofiles, mostly exposed on thermokarst mounds, consisting of still-frozen, undisturbed erosional remains of polygonal centres at the coastal bluff. Both profiles extend from sea level to the top of the cliff (Fig. 2). Additionally, deposits from a ther-

moerosional valley and from a thermokarst depression were studied. The subprofiles were labelled with the abbreviation “Mak” in the chronological order of field sampling (from Mak-1 to Mak-14).

The frozen sediments were described by colour, lithology, organic remains and cryostructures. Each subprofile was sampled at 0.5–1.0-m intervals. About 0.5–1 kg of frozen sediment was collected with a hammer or a small axe, and was then stored in sealed plastic bags. Additional samples were collected in aluminium boxes for field determination of the gravimetric ice content. The gravimetric ice content is determined as the ratio of the mass of ice in a sample to the mass of the dry sample (and is expressed as a percentage) (van Everdingen 1998).

All sediment samples were freeze-dried (Christ ALPHA 1–4) in the laboratory, and were carefully homogenized manually, without destroying the grain size, and finally were split into equal parts for the various analyses. A laser particle analyser (Coulter LS 200) was used to measure the grain-size distribution. Samples were treated with hydrogen peroxide before grain-size analysis to remove organic matter. The mass-specific mineral magnetic susceptibility (MS) was determined with an MS meter (Bartington MS2) with the sensor type MS2B. The values of MS are expressed in SI units ($10^{-8} \text{ m}^3 \text{ kg}^{-1}$). The contents of total organic carbon (TOC), total carbon (TC) and nitrogen (N) were measured with a CNS analyser (Elementar vario EL III). Stable carbon isotope ratios ($\delta^{13}\text{C}$) of TOC were measured with a Finnigan DELTA S mass spectrometer.

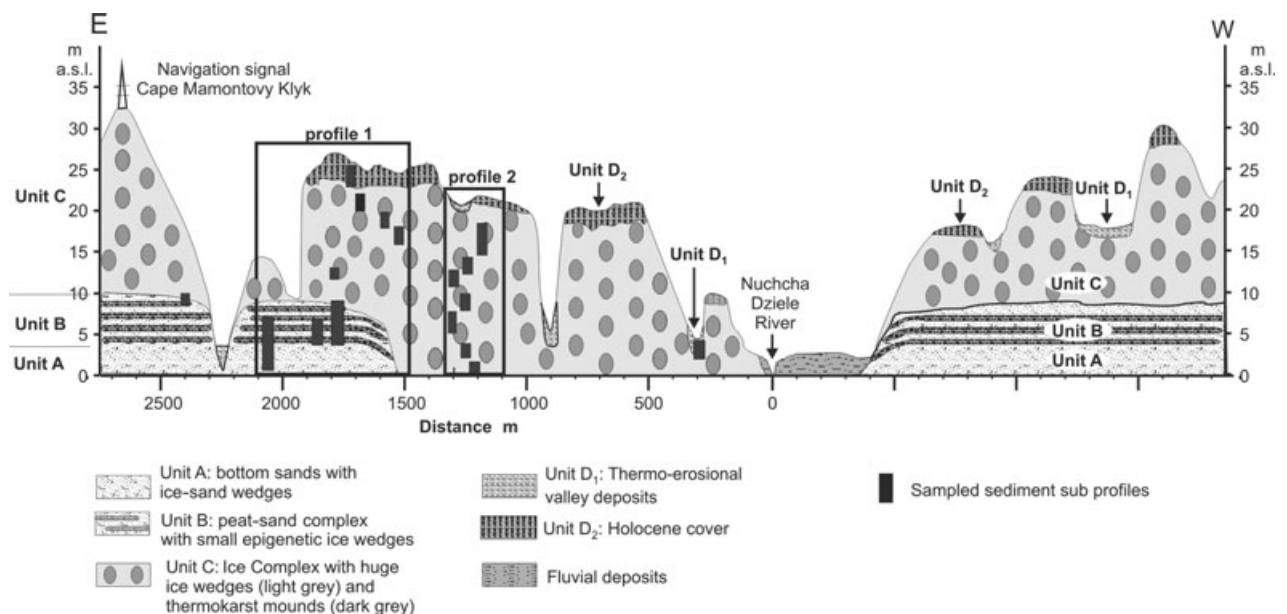


Fig. 2 General stratigraphic scheme of the main section of Cape Mamontov Klyk, with positions of both composite profiles 1 and 2, and location of the subprofiles. The exact arrangement of the subprofiles discussed in the paper is shown in Fig. 4.

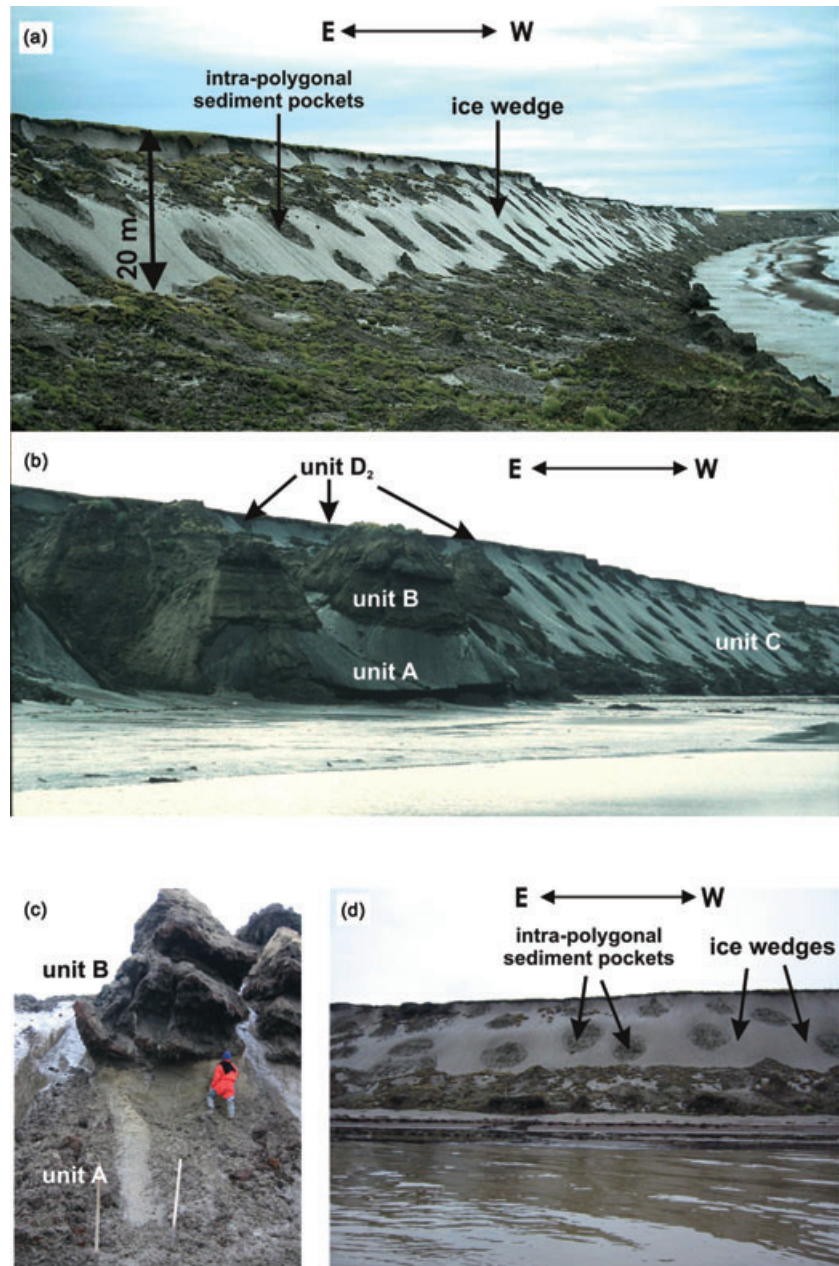


Fig. 3 The cliff of Cape Mamontov Klyk. (a) Ice wedges (light grey) and intrapolygonal sediment pockets (dark grey) on the Laptev Sea coast at Cape Mamontov Klyk. (b) Left, the sand unit A (lower part of profile 1); right, the Ice Complex unit C (profile 2 location). (c) Sand unit A and the above-lying peat sand alternation of unit B (subprofile Mak-1, position of the optically stimulated luminescence dated sequence). (d) The ice cliff of profile 2 (Ice Complex unit C, position of the subprofiles Mak-12, -13 and -15–19) exposes a diagonally cut fossil ice-wedge system. The dark grey, frozen sediment fillings of polygon centres are surrounded by the light grey ice of the ice wedges.

Heavy minerals were analysed on the 63–125 μm sub-fraction. The heavy minerals were separated using sodium metatungstate solution with a density of 2.89 g cm^{-3} . The mineralogical composition was analysed on microscope slides under polarized light. About 300–400 grains of each sample were counted. The mineralogical composition was calculated in grain percentages.

Selected organic material was dated using the accelerator mass spectrometry (AMS) facilities at the Leibniz Laboratory for Radiometric Dating and Stable Isotope Research (Kiel University, Germany). The Leibniz Labo-

ratory reduces the background that is inherent to the spectrometer, which results in low background count rates of the detector, equivalent to an apparent age of 75 Ky (gated background) (Nadeau et al. 1997; for details of the Leibniz Laboratory AMS procedures, also see Nadeau et al. 1998.)

The sediment ages of three samples from section Mak-1 have been determined using optically stimulated luminescence (OSL) dating (Aitken 1998). Quartz in the 100–150- μm fraction was analysed. Determinations of dose-rate relevant elements (K, Th and U) were carried

Table 1 Summary of optically stimulated luminescence (OSL) dating. The number of aliquots measured for each individual sample (*n*), the concentration of elements relevant for dose rate determination (K, Th and U), assumed average water content during burial (*W*), sample depth below surface, dose rate (*D*), the ratio of mean/median as indicator for normal Gaussian distribution of the individual measured palaeodose values (*D_E*), the mean and standard error of these measurements and the resulting OSL age are listed.

Sample	<i>n</i>	Grain size (µm)	K (%)	Th (ppm)	U (ppm)	<i>W</i> (%)	Depth (m)	<i>D</i> (Gy kyr ⁻¹)	Mean/ median	<i>D_E</i> (Gy)	Age (Ky)
MAK1	19	100–150	2.28 ± 0.20	5.32 ± 0.11	1.53 ± 0.07	35 ± 10	30.0	2.12 ± 0.28	1.01	120.0 ± 7.3	56.6 ± 8.3
MAK2	23	100–150	2.21 ± 0.20	4.07 ± 0.09	1.16 ± 0.05	35 ± 10	28.5	1.96 ± 0.24	0.98	61.2 ± 5.1	31.3 ± 4.6
MAK3	23	100–150	2.21 ± 0.20	5.65 ± 0.12	1.39 ± 0.06	35 ± 10	27.2	2.08 ± 0.26	1.04	66.3 ± 3.5	31.8 ± 4.3

out by inductively coupled plasma mass spectroscopy (ICP-MS) (Preusser & Kasper 2001). Water (ice) content was measured from sediment surrounding the samples. All samples investigated here are close to water saturation because they have been taken from permafrost. We used the average measured ice content (35%) and added 10% uncertainty to include possible past changes in the moisture content of the samples (Table 1). The contribution from cosmic radiation to the total dose rate was calculated following the method described by Prescott & Hutton (1994) using the present-day depth (ADELE software; Kulig, 2005). The palaeodose (*D_E*) was measured using the single aliquot regenerative dose (SAR) protocol (Murray & Wintle 2000), applying a preheating of 230°C for 10 s and a cut-heat to 160°C. This procedure has been cross-checked by several tests, as explained by Wintle & Murray (2006). For each of the samples, 24 small (2-mm) aliquots were measured, and the majority of those passed the criteria (e.g., recycling) suggested by Murray & Wintle (2000).

The possible incomplete bleaching of OSL prior to deposition could have been inferred from the distribution pattern of individual *D_E* values. The samples under consideration here are all normally distributed, as indicated by mean/median ratios close to unity. These ratios would be significantly greater than 1.00 for incompletely bleached samples (Preusser et al. 2007). Furthermore, the standard deviation of the whole set of individual *D_E* values is about 25%, and is hence within the magnitude observed for other samples that were considered to be well bleached. These observations imply full bleaching of OSL prior to deposition, and standard errors have been used for the calculation of the mean palaeodose (Table 1).

A standard hydrofluoric acid (HF) technique was used for pollen preparation (Berglund & Ralska-Jasiewiczowa 1986). The relative frequencies of pollen taxa were calculated from the sum of the terrestrial pollen taxa. Spore percentages are based on the sum of pollen and spores. The relative abundances of reworked taxa (Tertiary spores and redeposited Quaternary pollen) are based on the sum of pollen and redeposited taxa, and the percentages of algae are based on the sum of pollen and algae.

TILIA/TILIAGRAPH software (E. Grimm 1991, Illinois State University, Springfield, IL, USA) was used for the calculation of percentages and for drawing the diagrams.

For the analysis of plant macro-remains, bulk samples, which had previously been conserved by freeze-drying, were suspended in water and wet-sieved through a 250-µm-mesh screen. After drying, the sieving residues were examined for their macro-fossil content using a binocular microscope. The mass of sample material used depended on its availability, and varied between 30 g for peat (which has a large volume/mass ratio) and 200 g for minerogenous material. After picking, plants were identified by comparison of plant remains with modern reference material, both herbarium and carpological material. The environmental interpretation of macro-fossil records is based on modern ecology and the geographical distribution of the proven plant species, as described in Dierßen (1996), Möller (2000), Tolmachev (1995, 1996, 2000) and Malyshev & Peschkova (2003). To be consistent with modern vegetation, the reconstructed syntaxa follow the international phytosociological nomenclature (Weber et al. 2000). The reconstruction of syntaxa was carried out at class level, because the incompleteness of the fossil floral spectra made a finer taxonomical resolution impossible.

All mammal bones and fragments were collected, registered and identified during fieldwork in 2003 (Kuznetsova 2004). The collected bones were divided into five groups according to their location type. The first group contains bones that were found strictly in situ. For the second group of bones we know the altitude of the find, i.e., the level of minimum height of the original position of the bones. This makes it possible to define the area from which the bones come from. The third group contains bones that were found in the exposure, but either in or on debris flows. Bones in the fourth group were collected on the shore directly below the studied section. The latter group includes all bones collected on the small part of the shore near the mouth of the Nuchcha Dzhielle River. Selected bones were dated at the Radiocarbon Laboratory of the Geological Institute in Moscow.

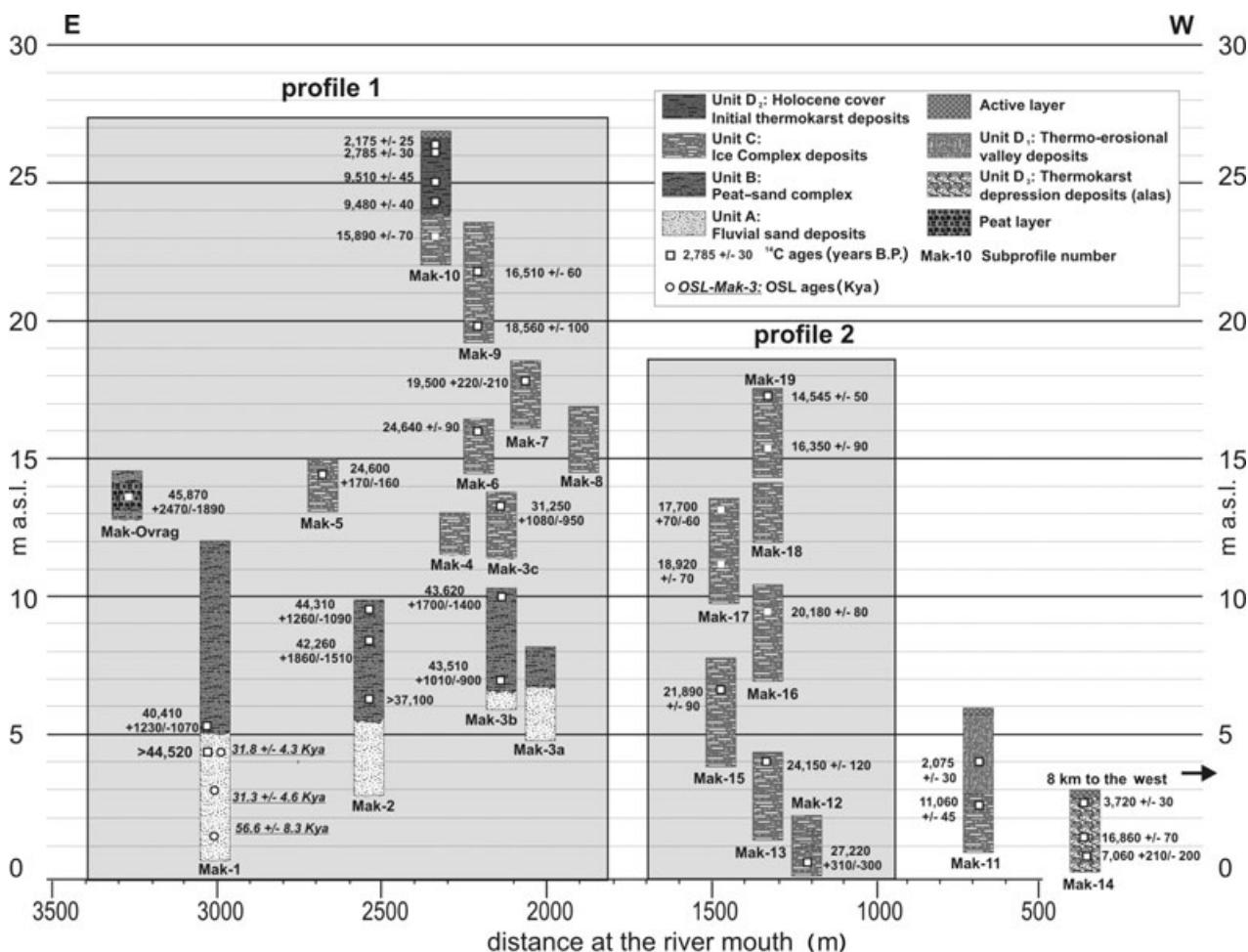


Fig. 4 Position, distribution and lithostratigraphy of the studied subprofiles from Mak-1 to Mak-14, sample position and results of optically stimulated luminescence (OSL), and radiocarbon accelerator mass spectrometry (AMS) age determinations.

Results

Local stratigraphy, cryostrutures and sediment characteristics

The studied coastal section is 2.2-km long and is situated between the Nuchcha Dzhihle River mouth and a deep thermoerosional ravine to the east (Fig. 2). The coast is characterized by steep bluffs (Fig. 3a) that erode into Yedoma hills. These are intersected by the Nuchcha Dzhihle River valley and its alluvial terraces, by several flat-bottomed thermoerosional valleys and by narrow but deep thermoerosional ravines. The exposure is divided into four main units, A–D, based on sedimentological and cryolithological characteristics (Fig. 2). The subprofiles of the main section were grouped into two composite profiles. Profile 1 includes the units A–D₂, whereas profile 2 consists solely of unit-C deposits (Fig. 2). Unit C extends from sea level up to 20–25 m a.s.l. between 500 and

1500 m east of the Nuchcha Dzhihle River mouth. This central part of the section is flanked to the west and the east by deposits of units A and B outcropping up to 10 m a.s.l. (Figs. 2, 3b). An additional section was studied in a thermokarst depression about 8 km west of the main exposure (Figs. 1b and 4).

Unit A. The lowest unit A (0–5 m a.s.l. in Fig. 4, profile 1 in Fig. 3c) consists of yellowish-grey, irregularly laminated fine-grained sand, without visible plant remains. The sands contain thin, light-grey, coarsely grained interbeds. The cryostruture is massive (i.e., no segregated ice is visible), and the gravimetric ice contents range from 25 to 40% by weight (Fig. 5). Many composite sand–ice wedges (subvertically streaky sand–ice alternations) were formed within unit A. Additionally, the sand unit was penetrated from above by large ice wedges of 2–3 m in width, and by a few small ice wedges (about 0.2–0.5 m in

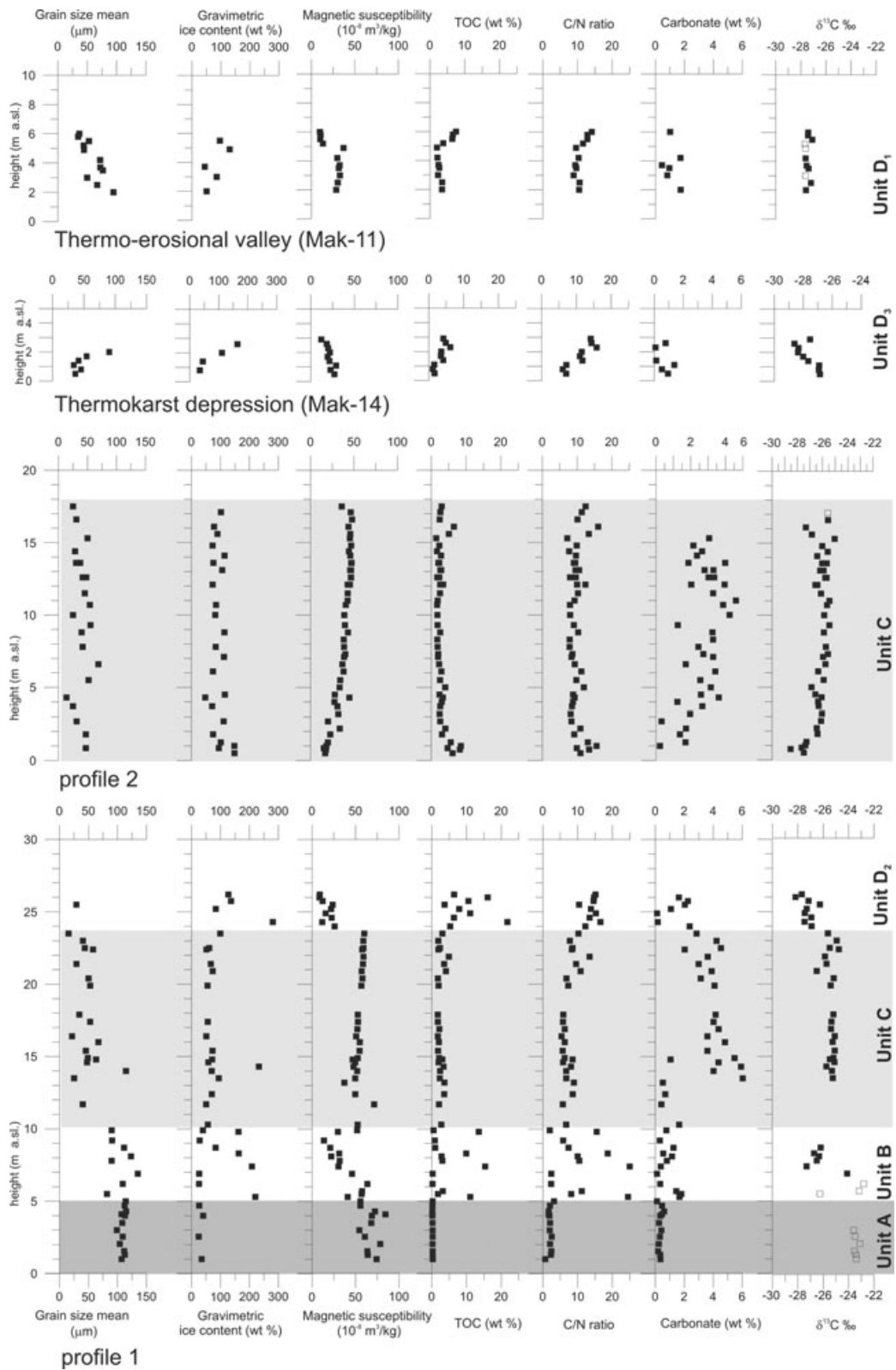


Fig. 5 Sediment characteristics of composite profiles 1 and 2, and of sections in a thermoerosional valley (Mak-11) and a thermokarst depression (Mak-14).

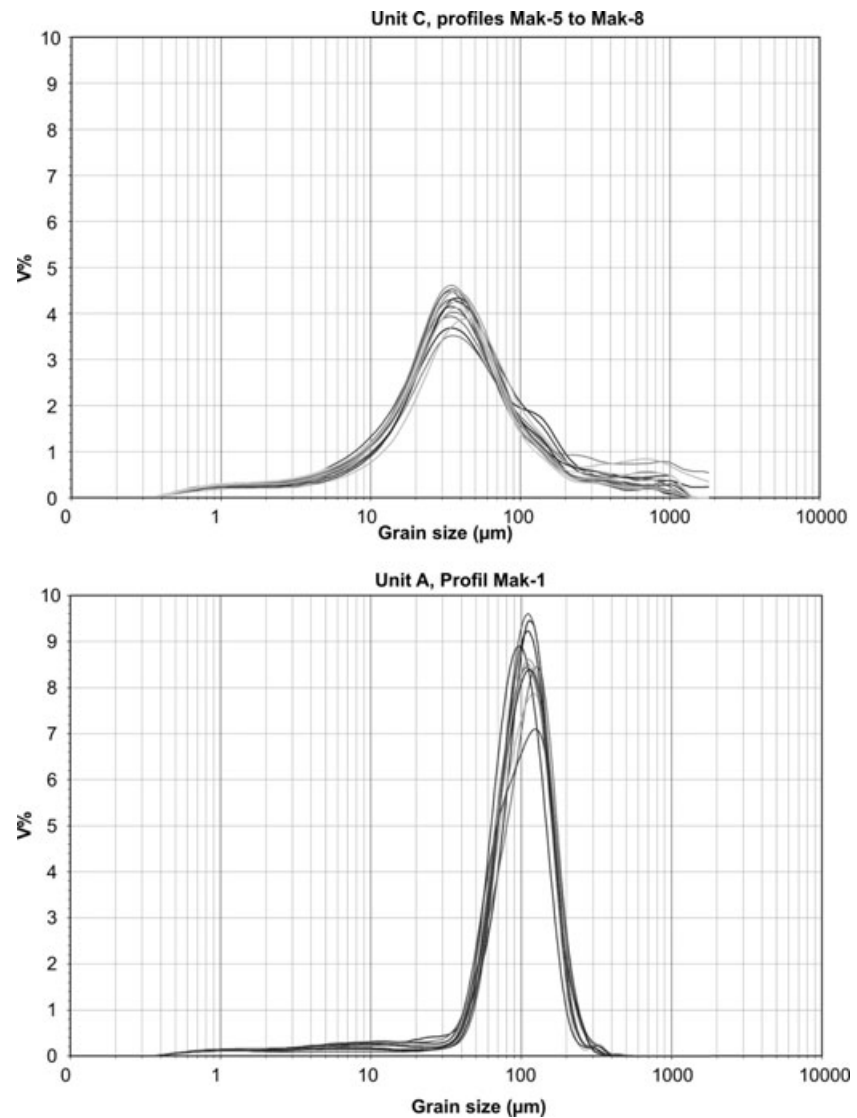


Fig. 6 Grain-size distribution pattern of organic free clastic matter in Ice Complex unit C and sandy unit A.

width). A transition zone of about 1-m thickness, containing numerous vertically oriented in situ grass roots, covers the organic-free sands. The cryostructure there is characterized by individual thin horizontal ice laminae and small vertical ice veins along grass root remains.

The sand unit A is characterized by a mean grain size of about 110 μm and the highest magnetic susceptibility (70–80 SI), as well as by the highest (heaviest) $\delta^{13}\text{C}$ values (from -23.2 to -24.0‰), of the studied sequences (Fig. 5). The $\delta^{13}\text{C}$ values are typical of aquatic plant matter. TOC (ca. 0.3% by weight), carbonate concentrations (ca. 0.4% by weight) and the C/N ratio (0.7–2.5) are very low. The homogeneous sediment parameters of unit A, and the narrow, medium-grained sand grain-size distribution (Fig. 6), attest to the stable and continuous accumulation conditions of a fluvial system.

Unit B. The overlying unit B (5–11 m in profile 1, Fig. 4) consists of an alternation of four cryoturbated peat-rich horizons, and irregularly laminated, dark-grey silty to fine-grained sandy interbeds (Fig. 3b,c). The peaty horizons mostly consist of brown moss peat inclusions of 0.2–0.5 m in diameter. They are generally supersaturated with ice (gravimetric ice content 160–220% by weight). The sediment directly below the peat-sand complex is brownish to reddish mottled, and appears to be a buried oxic gley-soil horizon. The dark grey silty sand interbeds contain large quantities of fine-distributed plant detritus and larger plant remains, such as grass roots and twig fragments. Diagonally oriented black, patchy non-regular stripes rich in organic residues cross the interbeds, caused by infiltration of organic matter. Net-like dark-brown sediment structures were

observed in interbed layers of the sub-profile Mak-2 that resemble synsedimentary water-escape structures of instable water-supersaturated sediments. The sandy interbed sediments are ice-rich (gravimetric ice content 26–83% by weight), and have a banded cryostructure (0.5–1-cm thick ice bands). Various generations of small ice wedges were observed within unit B, and can be assigned to individual peaty horizons. The thin ice wedges penetrated into the underlying unit A.

Alternating TOC values (1–15% by weight) and C/N ratios (6–25) reflect the observed peat–sand interbedding. Sandy interlayers have a mean grain size of 80–135 μm (Fig. 5). The magnetic susceptibility shows a clear trend towards lower values (60–14 SI) with increasing height, which probably mirrors gradual changes in the sediment composition, i.e., of the sediment source.

Unit C. The transition from unit B to unit C exposed in profile 1 is gradual. Unit C represents the ice-rich permafrost deposits of the Ice Complex (Fig. 3d), with their typical large ice wedges reaching from about 25 m a.s.l. down below the sea level in some locations. The Ice Complex deposits exposed between 11 and 24 m a.s.l. in profile 1, and between 0 and 17.5 m a.s.l. in profile 2, are composed of alternating mineral-rich (greyish) and organic-rich (brownish) sediment layers (each about 0.2–0.7 m thick). The brownish-coloured horizons contain higher quantities of visible plant fragments, peat inclusions, fine-grained plant detritus and mottled iron oxide impregnations. Such sequences were already described as buried cryosols (e.g., Schirrmeister, Siegert, Kunitsky et al. 2002; Schirrmeister, Siegert, Kuznetsova et al. 2002; Schirrmeister et al. 2003). Based on the content of peat and plant material, we subdivide unit C into two sub-units. The lower horizon of about 0–2 m a.s.l. in profile 2 (subprofile MAK-12; Fig. 4) consists of cryoturbated peat soils with silty to fine sandy interbeds. The upper and main part of unit C is formed by several weakly developed buried cryosols and silty to fine-grained sandy interbeds, with in situ grass roots, fragments of shrub twigs and leaves, and fine-detritus plant matter. The gravimetric ice content of unit C varies between 50 and 100%, by weight, for interbeds, and between 100 and 250%, by weight, for cryosol horizons, reflecting the typical ice supersaturation of such permafrost deposits. The cryostructure of the sediment is banded with lens-like reticulation between ice bands.

The deposits of unit C are mainly characterized by a uniform magnetic susceptibility of 50–60 SI, except for the lowermost peaty horizons (Fig. 5). The mean grain size usually falls between 25 and 50 μm . The carbonate contents are substantially higher (2–6% by weight) than in all other units. The TOC, C/N and $\delta^{13}\text{C}$ values are

rather similar in both composite profiles. The minor variations of these parameters reflect the occurrence of cryosols within the sequences. Changes in $\delta^{13}\text{C}$ values are caused by changes in organic matter provenance (i.e., plant remains and/or the decomposition of organic matter). The grain size distribution patterns of unit C are relatively wide (i.e., poorly sorted; Fig. 6), contradicting a pure aeolian genesis (loess). However, aeolian processes are very likely to have been involved in providing sediments for these deposits. The similarity between grain size distributions of various samples in the Ice Complex indicates a continuity of the same sedimentary processes during the accumulation.

Unit D. In places, unit C is discordantly covered by a 2-m thick sequence (unit D₂, 24–26 m a.s.l. in profile 1) of cryoturbated peat soil horizons (Fig. 3a), with loamy interbeds that represent the filling of small thermokarst ponds and polygonal ponds that developed on top of the Ice Complex (Yedoma hills). At the Yedoma surface these fillings usually appeared as irregularly distributed peat patches (10–50 m in diameter). The sediments of these small thermokarst-like depressions contain thin (<1-m width) white ice wedges. Unit D₂ is very ice-rich (gravimetric ice content 84–136% by weight), and the cryostructure is ice-banded and lens-like.

Additionally, unit D includes deposits of thermoerosional valleys (unit D₁) that discordantly cover the Ice Complex deposits of unit C in these narrow valleys. The lower part of our unit-D₁ profile (MAK-11; Fig. 4) contains two greyish-brown palaeo-sol, with peat inclusions and small ground wedges of about 10 cm in depth. The cryostructure is banded, partly massive or lens-like reticulated. The gravimetric ice content amounts to about 50%, by weight. The upper part of this profile consists of greyish-brown, well-bedded silty fine-grained sand, with some vertically oriented grass roots. It also contains wood fragments and peat inclusions. The cryostructure consists of ice bands and fine, sometimes broken, ice lenses (gravimetric ice content 46–130%, by weight).

Deposits in the thermokarst depression that belongs to unit D₃ (subprofile MAK-14; Fig. 4) were studied in a remote alas depression (about 8 km west of the Nuchcha Dzhihle River mouth). The sequence is composed of three parts. The lowest exposed 1 m of sediment consists of clayish fine-sandy silt with plant detritus, and is brownish in colour. The cryostructure is coarse lens-like and the gravimetric ice content is about 30%, by weight. This part is covered by a horizon of interbeddings of 2–3-cm-thick peat layers and sandy silt layers. Thin ice bands also occur. The gravimetric ice content varies between 45 and 110%, by weight. A cryoturbated peaty palaeosoil completes the sequence. The cryostructure is characterized by thick ice

belts and vertical ice veins (gravimetric ice content 165%, by weight).

The cover of unit D₂ contrasts obviously with the underlying Ice Complex deposits, especially in terms of magnetic susceptibility (26–8 SI) and $\delta^{13}\text{C}$ values (from –27.3 to –28.5‰). Lower (lighter) $\delta^{13}\text{C}$ values are also typical for the Holocene deposits in the thermokarst depression (unit D₃) and the thermoerosional valley (unit D₁).

Geochronology

The three calculated OSL ages are 56.6 ± 8.3 , 31.3 ± 4.6 and 31.8 ± 4.3 Ky (Table 1; Fig. 4). Whereas the first age fits well with the radiocarbon chronology of the sequence, the upper two samples are significantly younger. Assuming that the radiocarbon estimates are correct implies that the upper two OSL ages are underestimated. Changes in sediment moisture cannot account for the underestimation, as water saturation was assumed for the samples, and lower water contents will result in even younger OSL ages. Another explanation would be radioactive disequilibrium, but those are restricted to the uranium decay chain. Although information about radioactive equilibrium is not available for the present samples because not enough material was available for gamma spectrometry, the nature of the sediment and the environmental conditions (permafrost) make significant losses of daughter isotopes of uranium unlikely. Furthermore, the concentration of uranium is so low that it accounts for only a small percentage of the total dose rate (<10%). Assuming a 100% loss of uranium daughter isotopes would not increase the ages to more than 36 Ky. Alternatively, one could speculate about the instability of the quartz OSL in this particular region, but all OSL decay curves are dominated by fast components that are considered to be stable. Furthermore, this would also be in contrast to previous experience in the region that indicates that OSL dating does not underestimate Eemian sediments by more than about 10% (Murray et al. 2007). In summary, we have an apparent age underestimation of the upper two OSL samples, but no reasonable explanation for it. It is therefore recommended that future work investigate samples from the area in more detail than was possible in this project.

The Early to Middle Weichselian age of unit A is also supported by an infinite radiocarbon age of >44.5 Ky, as determined from in situ grass roots from the transition zone between units A and B. It is assumed that unit A corresponds to the Zyryan cold period (stadial). According to five radiocarbon ages, the peat–sand alternation of unit B was formed at about 40–45 Kya (Table 2; Fig. 4). This horizon was formed during the Kargin interstadial

period. The height–age relationship (Fig. 7) of composite profile 1 reveals a relatively large gap in the radiocarbon age sequence between 40 and 24.6 Kya. The gradual transition to the ice-rich unit C is only evident in one date of 31.2 Kya. For both composite profiles in the Ice Complex (unit C), continuous radiocarbon AMS dates were found for the periods between 26.6 and 15.9 Kya and between 27.2 and 14.5 Kya. These indicate that the Ice Complex formed during the Sartan cold period. The well-correlated age–height relationship ($R^2 = 0.92$ and 0.98) in both composite profiles (Fig. 7) allows the estimation of accumulation rates between 14 and 15 mm per year for the Ice Complex formation. The early Holocene period was radiocarbon dated in the upper part of the composite profile 1 (unit D₂) at about 9.5 Kya, and was followed by late Holocene deposits (also unit D₂) between 2.7 and 2.1 Kya. Deposits from a thermoerosional valley (unit D₁ in subprofile Mak-11) were formed between 11 and 2 Kya. Four radiocarbon ages (Table 2) from sediments in a thermokarst depression (unit D₃) revealed age inversions. The dates ranged from 16.8 to 1.5 Kya, and probably indicate partial redeposition of older organic material into the thermokarst depression.

Heavy mineral analysis

The dominant heavy minerals in the permafrost sequences of Cape Mamontov Klyk are epidote, pyroxene and amphibole (Fig. 8), which are characteristic for crystalline metamorphic rocks. Grain morphology varies, but is mostly weakly rounded. The minerals are well preserved, except for epidote (often decomposed and altered) and micas (discoloured by iron oxide and fissured). Epidote occurs in both altered and fresh states. Well-formed prismatic crystals are rare. Sometimes epidote is coalesced with other minerals, e.g., zoisite. Rhombic pyroxenes are represented by hypersthene, and the clinopyroxenes are represented by diopside. Augites occur only as admixtures. The relationship between augite and diopside changes sometimes over short distances. Amphibole is usually represented by dark green hornblende. A small number of amphibole grains are colourless, grey-brown and bluish-green. Ilmenite, often altered to leucoxene, appears sometimes together with titanite. Titanite, frequently altered to leucoxene, is present in the form of prismatic and envelope-like crystals, but is more often found only as irregular fragments and aggregate grains. The colour of titanite grains ranges from light grey-brown to reddish grey-brown, with strong pleochroism. Tourmaline was found in the form of prismatic crystals and its fragments. The colour is grey-brown for Mg varieties and, more rarely, blue for Fe varieties. Garnets occur as irregular, non-rounded

Table 2 Radiocarbon accelerator mass spectrometer (AMS) dating results.

Lab. no	Sample	Description	Height (m a.s.l.)	¹⁴ C age (years B.P.)	Cal. ages B.P. (2σ)
KIA 25037	Mak-Ovrag-1	peat	15	45 870 +2470/–1890	
Profile 1					
KIA 25085	Mak 1-9	plant remains	4.3	>44 520	
KIA 23771	Mak 1-12	moss peat	5.3	40 410 +1230/–1070	
KIA 25086	Mak 2-1	plant remains	6.2	>37 100	
KIA 25087	Mak 2-6	peat inclusion	8.3	42 260 +1860/–1510	
KIA 23772	Mak 2-9	moss peat	9.8	44 310 +1260/–1090	
KIA 25088	Mak 3-7	moss peat	7	43 510 +1010/–900	
KIA 25089	Mak 3-14	wood fragments	10.3	43 620 1700/–1400	
KIA 23773	Mak 3-17	moss peat	13.2	31 250 +1080/–950	
KIA 25090	Mak 5-3	small steems	14.3	24 600 +170/–160	
KIA 25091	Mak 6-4	grass roots	16	20 640 ± 90	
KIA 25092	Mak 7-4	grass roots	17.9	19 500 +220/–210	
KIA 25093	Mak 9-1	plant fragments	19.9	18 560 ± 100	22 767–21 346
KIA 25094	Mak 9-5	twig fragments	21.9	16 510 ± 60	20 301–19 084
KIA 29831	Mak 10-2	plant remains	23	15 890 ± 70	19 259–18 387
KIA 25095	Mak 10-5	wood fragments	24.3	9 480 ± 40	10 789–10 633
KIA 29832	Mak 10-8	plant remains	25.2	9 510 ± 45	10 883–10 639
KIA 25096	Mak 10-11	peat	26	2 785 ± 30	2 950–2 839
KIA 29833	Mak 10-12	plant remains	26.2	2 175 ± 25	2 308–2 226
Profile 2					
KIA 25097	Mak 12-1	peat inclusion	0.5	27 220 ± 310/–300	
KIA 25098	Mak 13-7	twigs	4	24 150 ± 120	
KIA 25099	Mak 15-5	twigs	6.6	21 890 ± 90	
KIA 25100	Mak 16-5	twigs, plant remains	9.3	20 180 ± 80	
KIA 25101	Mak 17-3	twig fragments	11.5	18 920 ± 70	23 194–21 776
KIA 25102	Mak 17-7	plant fragments	13.5	17 700 +70/–40	21 705–20 415
KIA 25103	Mak 19-3	plant remains	15.3	16 350 ± 90	20 133–18 902
KIA 25104	Mak 19-7	twigs	17.1	14 545 ± 50	17 937–16 935
Thermo-erosional valley					
KIA 26107	Mak 11-2	plant remains	2.5	11 060 ± 45	13 187–12 876
KIA 25108	Mak 11-6	grass roots	4	2 075 ± 30	2 122–1 969
Thermokarst depression					
KIA 29834	Mak 14-2	plant remains	0.8	7 060 +210/–200	8 216–7 567
KIA 25109	Mak 14-4	plant remains	1.4	16 860 ± 70	20 715–19 458
KIA 29835	Mak 14-4	plant remains	1.4	1 480 ± 20	1 407–1 327
KIA 25110	Mak 14-8	moss peat	2.6	3 720 ± 30	4 151–3 979

angular fragments of rose colour, and are seldom of the grey-brown, orange and light-yellow varieties. Chlotitoide, disthene, staurolite, andalusite and sillimanite, typical minerals of metamorphic rocks, are ubiquitously present in small quantities.

The samples studied are quite similar in heavy mineral composition, as well as in grain shapes. No strong alterations were observed in 135 samples covering the entire exposed sequence. We conclude that no changes of the source material area occurred over the period of deposition. The source materials were mainly crystalline metamorphic rocks of the Anabar Shield.

Palynological results

The lowermost sediments (unit A) from Cape Mamontov Klyk were OSL and radiocarbon dated to between

56.2 ± 6.7 and >44.5 Kya, and contained no pollen grains, which suggests a fluvial origin.

The oldest radiocarbon-dated pollen spectra from Cape Mamontov Klyk, pollen zone I (PZ-I) of Fig. 9, corresponds with the uppermost grass root-bearing transition horizon of unit A. Pollen of Cyperaceae, Poaceae, and *Artemisia* and *Encalypta* spores dominate the spectra. PZ-I is characterized by high contents of green algae colonies of *Botryococcus* and especially *Pediastrum*, indicating the existence of shallow water accumulation conditions. The relatively high content of *Encalypta* spores in several samples point to disturbed soils. Aside from the sandy interbeds, PZ-I is dominated mostly by Cyperaceae and Poaceae pollen. It also contains rather numerous colonies of *Botryococcus*. The lowest sample (Mak12-1, 27.7 Kya) of Ice Complex unit C still belongs to PZ-I, suggesting that Ice Complex formation had already started at the end

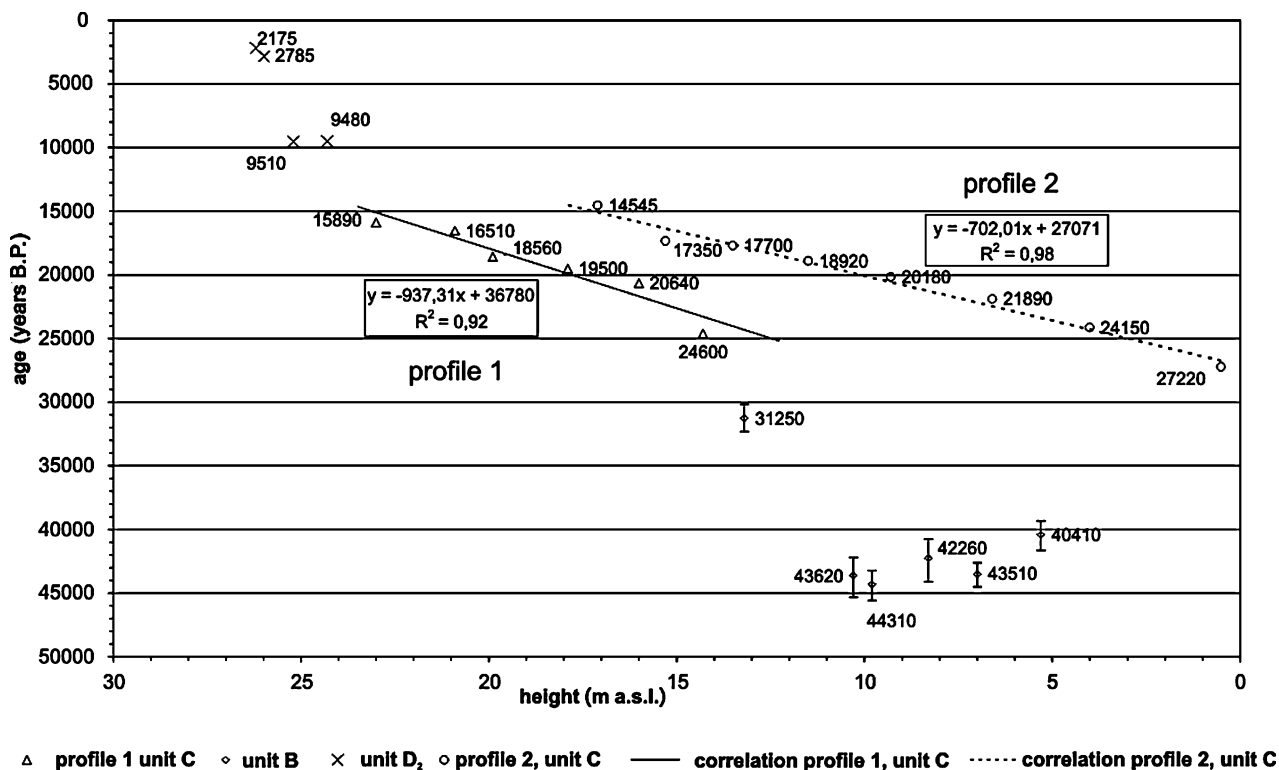


Fig. 7 Age–height relationships in composite profiles 1 and 2, and the linear trends within the Ice Complex sequence (unit C) at Cape Mamontov Klyk. The black line indicates the subprofiles from Mak-5 to Mak-10; the dotted line indicates Mak-12, -13, and -15–19.

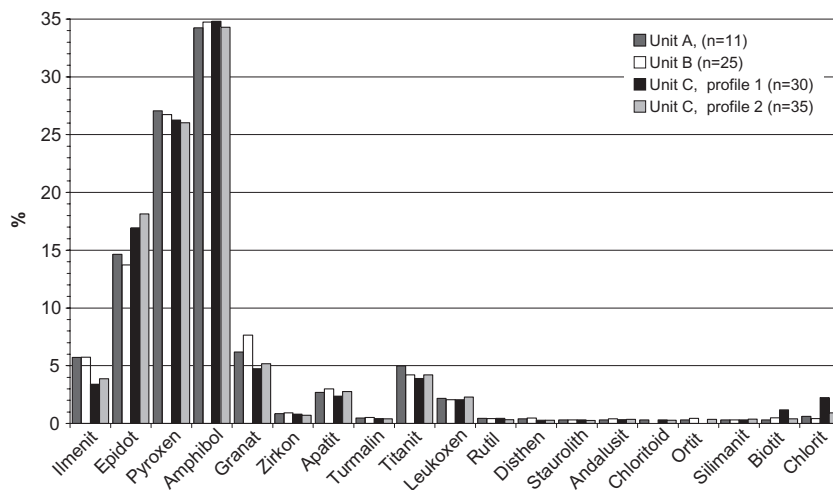


Fig. 8 Summary of the heavy mineral analysis of 101 samples of units A, B and C (profiles 1 and 2).

of the Kargin period. Dominance of Cyperaceae and Poaceae pollen with a few other herbs and *Salix* is typical for the sediments in the Laptev Sea region, and are radiocarbon dated to ca. 45–28 Kya (Andreev et al. 2002; Schirrneister, Siegert, Kunitsky et al. 2002; Schirrneister et al. 2003, and references therein). Thus, we can assume that pollen spectra from PZ-I reflect the open tundra- and steppe-like associations that dominated the area during

the Middle Weichselian (Kargin) interstadial. The Arctic climate was relatively humid and moderate compared with the next period.

PZ-II (ca. 24.5–14.5 Kya) from the Ice Complex unit C is dominated mostly by the pollen of Poaceae, with some Cyperaceae, *Artemisia*, Brassicaceae and Caryophyllaceae. This zone is also characterized by large quantities of green algae colonies, reworked Pinaceae (indicating

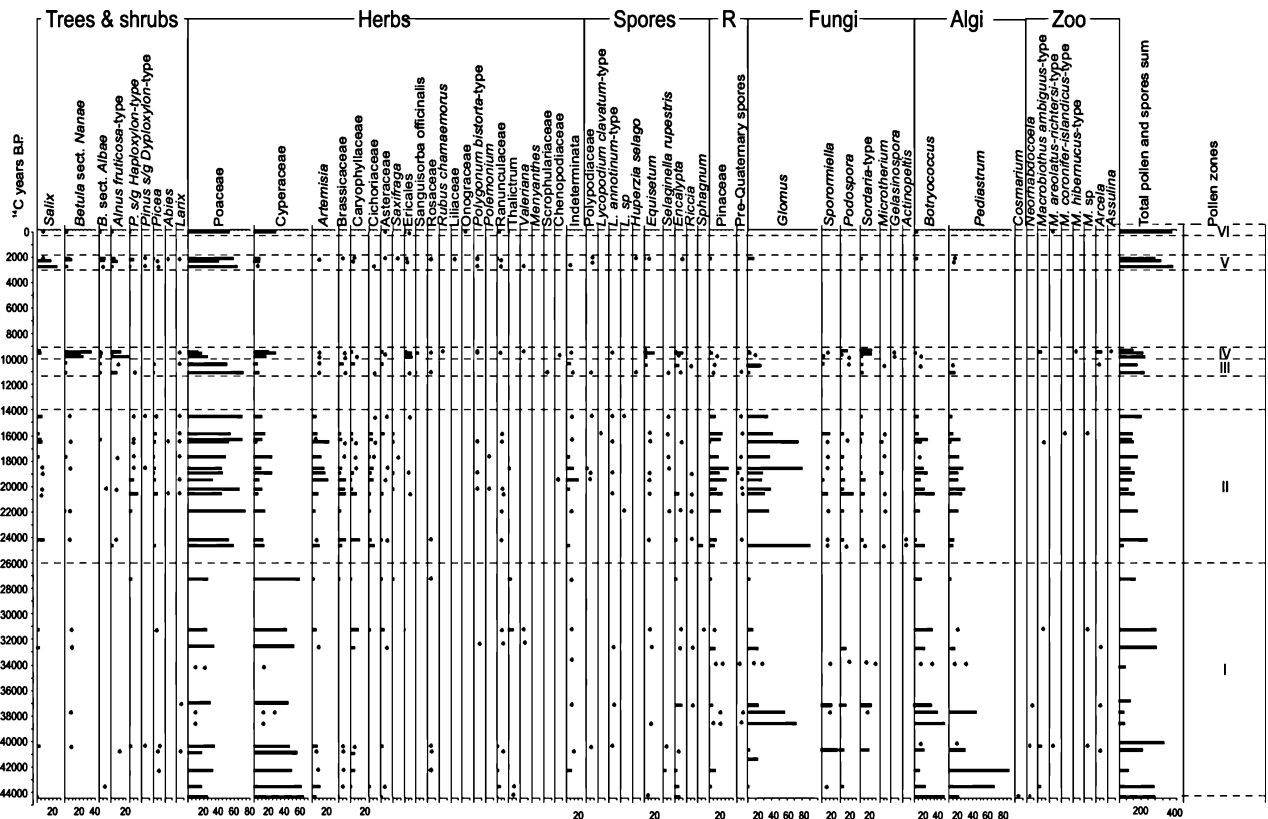


Fig. 9 Generalized composite pollen diagram of permafrost sequences at Cape Mamontov Klyk.

active erosion processes) and spores of fungi such as *Glomus* (indicating disturbed soils), and dung-habitat Sordariaceae (*Sporormiella*, *Podospora* and *Sordaria*). Pollen data indicate that open tundra- and steppe-like associations dominated the area during the Late Weichselian (Sartan). The climate was very cold and dry. However, a relatively high content of algae colonies in the sediments indicates that sedimentation occurred in shallow water bodies (e.g., ice-wedge polygon centres). Rather numerous dung-habitat Sordariaceae indirectly reflect the presence of grazing mammal herds in the area. Sediments radiocarbon dated to ca. 16.5 and 14.5 Kya contain higher amounts of *Salix* than the older sediments below, indicating wetter and warmer conditions after the Last Glacial Maximum (LGM). Similar changes were found in the eastern part of the Laptev Sea region (Bykovsky Peninsula; Andreev et al. 2002).

The lower pollen spectrum of PZ-III, radiocarbon dated to 11 Kya, originates from the lower part of the thermo-erosional valley sequence (unit D₁). This spectrum is dominated mostly by pollen of Poaceae, with some Cyperaceae, *Alnus fruticosus* and a few *Betula* sect. *Nanae*. A small peak of *Alnus* (11%) and the presence of *Betula* in the spectrum point to a relatively warm climate (e.g.,

alder is absent in the modern vegetation). Thus, the pollen spectrum reflects significant climate amelioration in the area, and can be correlated with the Allerød according to the radiocarbon date. Similarly dated pollen spectra from the eastern Laptev Sea coast (Grosse et al. 2007; Andreev et al., in press) are also characterized by rather large quantities of shrub pollen, and reflect the same climate amelioration. The upper pollen spectrum of PZ-III contains less shrub pollen, whereas Brassicaceae, Caryophyllaceae, Asteraceae and *Glomus* spore content are higher. The changes mirror the deterioration of the climate, which can be correlated with Younger Dryas cooling.

Early Holocene pollen spectra (PZ-IV) from the Holocene cover (unit D₂) on the top of the Ice Complex sequence were radiocarbon dated at around 9.5 Kya. The spectra are dominated mostly by pollen of shrubs (*A. fruticosus*, *Betula* and *Salix*) and semi-shrubs (Ericales), with some Cyperaceae and Poaceae. Spores of *Equisetum* and *Encalypta*, indicators of disturbed soils, are also common. The pollen spectra indicate that shrub-tundra vegetation was dominant, and that there was a significant amelioration in climate relative to the previous period. The high content of dung-inhabiting Sordari-

aceae spores indirectly reflects the presence of grazing mammal herds in the area. Late Holocene pollen spectra (PZ-V) from the uppermost part of units D₁ and D₂, radiocarbon dated to between 2 and 3 Kya, are dominated by the pollen of Poaceae and shrubs (mostly *Salix*). Such spectra reflect low shrub-tundra vegetation. The climate conditions were significantly colder than during the early Holocene. The surface pollen spectrum (PZ-VI) is dominated by Poaceae, with some Cyperaceae, and reflects the modern tundra environment in the area well.

Plant macrofossil results

All samples studied for plant macroremains originate from profile 1, which includes units A–D. Their composition was affected less by the macroclimate than by depositional conditions, which changed dramatically between the different facies. The two samples taken from the lowermost sandy unit A were completely free of identifiable plant remains. This results from the probable fluvial deposition regime. Running water tends to remove lightweight sediment fractions, including plant remains. The presence of macrofossils was thus affected less by macroclimate than by depositional conditions, which changed dramatically between the different facies. The available plant remains were altogether well preserved. Plant taxa could be identified mainly by very characteristic plant parts, such as seeds, fruits, buds and leaf fragments.

Plant fossil content and composition in unit B were also obviously affected by fluvial sedimentation, resulting in alternating sand–peat bedding that was likely to indicate the successive migration of a river branch and changing current velocities. Sandy samples in unit B were therefore also very poor in plant remains: usable material came mainly from the peaty interlayers. As expected from the depositional environment, the floristic composition in these samples was dominated by wetland plants, such as sedges and cotton grass (Table 3). The yellow marsh saxifrage (*Saxifraga hirculus*) was present exclusively in unit B. Although in low quantities, we also detected the remains of plants that are characteristic of upland habitats, including Kobresietea (abundant in individual samples: *Dryas* and *Kobresia myosuroides*) and Arctic pioneer communities (*Thlaspitea rotundifolii*). Only sub-Arctic shrubs were absent. This relative diversity in vegetation types, reflecting the presence of various, also dry, habitats, might be an indication of relatively dry and warm environmental conditions, superimposed with local wetness as a result of the periodical flooding from the nearby river.

As indicated by sediment characteristics and the homogeneous floral composition of plant remains, the taphonomic conditions remained constant within unit C, which is composed exclusively of Ice Complex deposits. According to the radiocarbon dating, unit C was deposited during the Last Glacial Maximum and the latest stage of the Weichselian glacial. In contrast to the other sedimentological units, the macrofossil assemblages in unit C are indicative of the macroclimate, rather than of local environmental conditions. The Ice Complex could only have been formed under very cold winter temperatures (i.e., during cold stages when the climate was extremely dry and continental). Plants typical of Arctic pioneer vegetation, and sporadic species of Kobresietea and steppe communities, were found (Table 3), thereby reflecting the existence of a tundra steppe with a cold and dry climate. In one late glacial sample, *Salix cf. arctica* remains were dominant: also an indicator of cold conditions.

The floral spectra changed dramatically towards unit D₂, which was separated from unit C by a hiatus. Unit D corresponds with the Holocene. The most characteristic features in the lower part of unit D were the presence and dominance of sub-Arctic shrubs and semi-shrubs, including *Betula nana*, *A. fruticosa* and *Empetrum nigrum*, clearly reflecting a drastically higher temperature than in unit C (Table 3). The abundance of water sedges (*Carex* sect. *Phacocystis*) indicates paludification, perhaps as result of thermokarst processes. Dryness indicators mostly disappeared in unit D, except for *Potentilla stipularis*, which was found in the lowermost sample Mak10-5.

Even within unit D, another drastic floral shift occurred. In the late Holocene sample 10–11, vascular plant remains were almost entirely absent, despite the peat substrate that consisted of moss remains. The only vascular plants that could be identified were *Salix*, *Luzula* and *Juncus* sp. These plants are resistant to cold temperatures and wet conditions, and indicate a large temperature drop compared with the Early Holocene and continuously wet conditions.

Results of fossil mammal studies

The taxonomic composition of the bone collection is typical for the mammoth fauna of Arctic Siberia (Fig. 10a). However, the percentages of various species differ. Reindeer bones are predominant (ca. 43%), in contrast to horse (ca. 33%), woolly mammoth (ca. 10.5%) and bison (ca. 5%). Such a low number of mammoth bones and large quantity of reindeer bones could be explained by taphonomic factors, and does not necessarily reflect the composition of mammal populations during the Late Pleistocene. The large number of

Table 3 Results of plant macrofossil studies.

		Unit B					Unit C				Unit D ₂			
Sample no.		1-12	2-6	2-8	2-9	3-14	3-17	6-4	7-4	9-4	10-1	10-5	10-7	10-11
Sample mass (g)		30	30	200	50	200	150	200	200	100	30	50	100	10
Substrate		peat	peat	sand	peat	sand	sand	silt	silt	silt	silt	peat	silt	peat
¹⁴ C dating (Kya)		42			43			20.5	19.5	16.5	9.5		2.8	
Snow beds (Salicitea herbaceae Br.-Bl. 1947)	<i>Salix cf. arctica</i>									180				
	<i>Salix</i> sp.	11	2								8	21		2
	<i>Saxifraga hieracifolia</i>												1	
	<i>Juncus biglumis</i>	11			6		5	4	1	38				
	<i>Juncus</i> sp.			3										1
	<i>Luzula</i> sp.			1										9
	<i>Luzula confusa</i>				1							3	2	
	<i>Potentilla hyparctica</i>		1								4	1		
	<i>Cerastium beeringianum</i>								13	7	1			
	<i>Cerastium jensejense</i>								47	5	1			
<i>Cochlearia arctica</i>											2			
<i>Draba</i> sp.	1							×100	170	13				
<i>Gastrolychnis involucreta</i> cf. <i>Lesquerella arctica</i>								6	3					
<i>Minuartia cf. stricta</i>	3			6						1				
<i>Minuartia rubella</i>						1	146	26	12	1				
<i>Stellaria cf. ciliatosepala</i>						2								
<i>Papaver</i> sect. <i>Scapiflora</i>		1			2		86	1	3					
<i>Saxifraga cespitosa</i>											2			
<i>Potentilla</i> sp.		2					35	5		2				
<i>Potentilla nivea</i>	1	1												
<i>Dryas</i> sp.				47		2				1				
<i>Kobresia myosuroides</i>	13													
<i>Pedicularis cf. labradorica</i>										3				
<i>Ranunculus affinis</i>						2								
<i>Thalictrum alpinum</i>				4		1								
<i>Artemisia</i> sp.						1		5						
<i>Artemisia</i> sp.						1		5						
<i>Alyssum obovatum</i>								1						
<i>Androsace septentrionalis</i>								1						
<i>Carex cf. duriuscula</i>	21		3			8				1				
<i>Elytrigia/Elymus</i> sp.														
<i>Festuca</i> sp.								1						
<i>Potentilla stipularis</i>						3						14		
<i>Poa</i> sp.								2	15	3				
<i>Puccinellia</i> sp.	1					1						1		
<i>Puccinellia tenuiflora</i>													1	
<i>Alnus fruticosa</i>													20	
<i>Betula nana</i> s.l.											69	58		
<i>Empetrum nigrum</i> s.l.													11	
<i>Ledum palustre</i> s.l.													2	
<i>Valeriana capitata</i>											1			
<i>Ranunculus borealis</i>													8	
<i>Caltha palustris</i>	4					5								
<i>Ranunculus lapponicus</i>													4	
<i>Carex</i> sect. <i>Phacocystis</i>			52		68	7					191	49		
<i>Epilobium davuricum</i>					1									
<i>Epilobium</i> sp.	4													
<i>Eriophorum brachyantherum</i>					5								1	
<i>Eriophorum russeolum</i>	1													
<i>Eriophorum scheuchzeri</i>					1									
<i>Gastrolychnis violascens</i>														
<i>Saxifraga hirculus</i>			1		7	2								
<i>Asteraceae</i> sp.					3									
<i>Carex</i> sp.	37											16	2	
<i>Cyperaceae</i> sp.													6	
<i>Poaceae</i> sp.			2					1		3		4		

Plant macrofossil record of the Cape Mamontov Klyk permafrost sequence and reconstructed plant communities (Syntaxa) according to the present day main occurrences of the identified plant taxa. Dotted lines indicate that some plants may occur in several communities. ×100 = several hundred individuals.

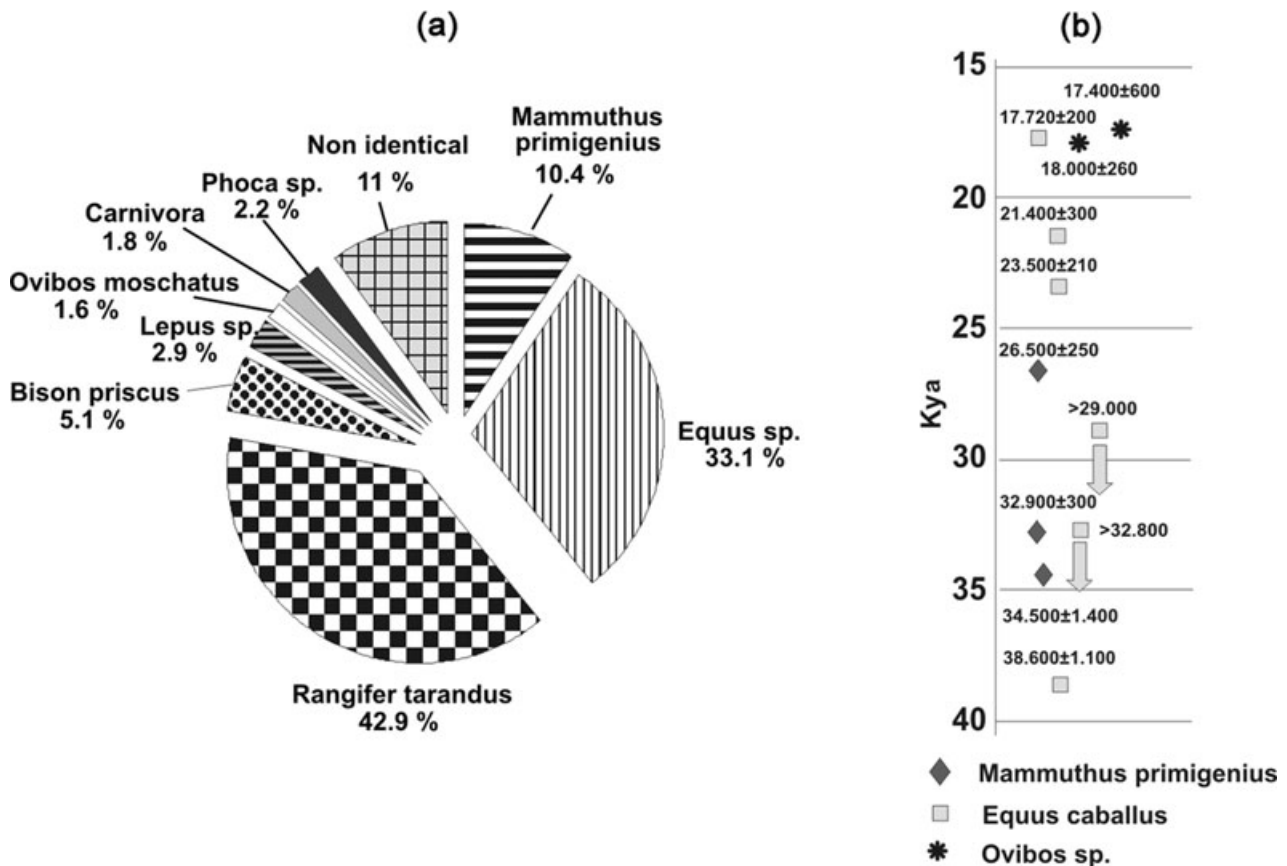


Fig. 10 Results of palaeontological studies. (a) Composition of mammal bone collection from the Olenek–Anabar region, Cape Mamontov Klyk (total number 501 samples). (b) Age distribution of radiocarbon-dated mammal bones collected from Cape Mamontov Klyk.

reindeer bones probably involved both fossil and modern reindeer bones. The preservation of all bones is typical for Ice Complex sites. They are very well preserved, and often have light-coloured, smooth outer surfaces and fragments of marrow inside the bones. Each bone has a white colour at the chip. Therefore, modern bones on the shore are not easily distinguished from fossil bones.

Most of the bones (80%) were collected on the shore near the mouth of the Nuchcha Dzhielle River. This collection consists of small bones, bone fragments and the teeth of hooved animals that were washed up by the river. However, large limb bones and teeth of woolly mammoth were absent at that site.

Only 20% of the collection was found directly in the exposures and on the shore in front of them. Eight bones were found strictly in situ in Ice Complex deposits. Three bones (tusk, thigh and thoracic vertebra) from this group probably belong to one woolly mammoth individual that lived $34\,500 \pm 1\,400$ years B.P. Another in situ woolly mammoth bone (thigh) was dated to $26\,500 \pm 250$ years B.P. Both dated samples were found at about 10–12 m a.s.l.

Nearly 20 samples that belong to the second and the third group were also found within the exposure, but not in situ. Samples (tusk, thigh and thoracic vertebra) of the first and the second group are important for the geological interpretation. In contrast to the taxonomical percentages for the whole collection (Fig. 10a), the composition of the first three groups is rather typical for the mammoth fauna. Fossil remains of woolly mammoth (ca. 25%), horse (ca. 30%) and reindeer (ca. 33%) are dominant.

A fourth group of nearly 70 samples includes bones that were collected on the shore in front of the exposure. The majority of the bone collection comes from the small area near the mouth of the Nuchcha Dzhielle River: 395 samples. Bones in this group were indubitably sorted and rounded by fluvial transport. This group has a completely different type of preservation, with many small scratches, cracks and a dark colour, not only on the outside, but also on the inside of the bone. The species composition of this group differs from the exposure bone collection. The number of reindeer bones (ca. 47.5%) is significantly higher than the number of mammoth bones (ca. 9.5%).

Table 4 Radiocarbon dating of mammal bone. Location types: 1, in situ; 2, in the exposure; 3, shore, in front of the exposure; 4, shore, river mouth.

No.	Sample no.	Taxon	Skeleton element	Preservation	Loc. type	Locality	GIN no.	C ¹⁴ years B.P.
1	MaK-O 31	<i>Mammuthus primigenius</i>	tooth	fragment	3	shore, east side below the navigation signal	GIN—13232	32 900 ± 300
2	MaK-O 91	<i>Mammuthus primigenius</i>	femur	damaged (4 pieces)	1	in situ, exposure, unit B, altitude 10–12 m a.s.l.	GIN—13220	26 500 ± 250
3	MaK-O 105	<i>Equus caballus</i>	tibia	fragment	2	exposure, right side, sand deposits	GIN—13249	23 500 ± 210
4	MaK-O 156	<i>Equus caballus</i>	femur	fragment	4	shore, mouth of Nuchcha Dzhielle River	GIN—13238	>29 000
5	MaK-O 194	<i>Equus caballus</i>	cervical vertebra	damaged	3	shore, east side in front of the Ice Complex outcrop	GIN—13247	>32 800
6	MaK-O 204	<i>Equus caballus</i>	crania (occipitale)	fragment	4	shore, mouth of Nuchcha Dzhielle River	GIN—13257	17 720 ± 200
7	MaK-O 207	<i>Ovibos</i> sp.	humerus, left	distal fragment	4	shore, mouth of Nuchcha Dzhielle River	GIN—13264	18 000 ± 260
8	MaK-O 214	<i>Equus caballus</i>	femur	fragment	4	shore, mouth of Nuchcha Dzhielle River	GIN—13251	21 400 ± 300
9	MaK-O 225	<i>Equus caballus</i>	humerus, left	fragment	4	shore, mouth of Nuchcha Dzhielle River	GIN—13246	38 600 ± 1 100
10	MaK-O 329	<i>Ovibos</i> sp.	cervical vertebra	damaged	4	shore, mouth of Nuchcha Dzhielle River	GIN—13243	17 400 ± 600
11	MaK-O 478	<i>Mammuthus primigenius</i>	tusk	fragment (3 pieces)	1	in situ, exposure, unit B, (2nd peat layer), 10 m a.s.l.	GIN—13219 (1 piece)	34 500 ± 1 400

The radiocarbon dating of bones completes our taxonomical study. We have 11 radiocarbon dates (Table 4; Fig. 10b): three dates from woolly mammoth bones, six dates from horse bones and two dates from musk ox bones. The radiocarbon dates lie between 39 and 17 Kya.

Discussion

Based on our field observations and laboratory analyses, we conclude that significant facies changes occurred in the study area during the considered late Quaternary period, and that these changes were probably related to broader environmental changes (Fig. 11).

The lowermost sand unit A was deposited in a hydrological system of higher transport energy compared with units B and C. We assume that a river branch was the likely accumulation environment for unit A (Fig. 11a). The lack of variations in sediment over the whole deposition period point to rather uniform environmental conditions. Similar sand horizons were widely distributed along the coast west and east of Cape Mamontov Klyk. Sandy deposits similar to unit A were also described further inland near the Pronchishchev Ridge, and along the Urasalakh River valley (Bolshiyarov & Makarov 2004). According to data from a drilling transect stretching from the cliff near Cape Mamontov Klyk out north onto the Laptev Sea shelf (about 12 km), this sand continues at more than 10 m below the sea level

(Overduin et al. 2007). Based on this evidence, a river-dominated landscape is reconstructed for the Zyryan period (corresponding to Early Weichselian cold stage, and to marine isotope stage 4 [MIS 4]), when fluvial sand sequences accumulated in the study area in front of the Pronchishchev Ridge (Fig. 11a). A fluvial sedimentation regime is unfavourable for the deposition and preservation of organic matter. Potential bioindicators are therefore scarce in unit A. The lack of organism remains makes the reconstruction of environmental conditions difficult. Similar palaeoriver conditions have been described further east along the Chekanovsky Ridge in the western Lena Delta (Schirrmeister et al. 2003; Wetterich et al. 2008), and in front of the Kharaulakh Ridge at Bykovsky Peninsula, south-east of the Lena Delta (Siegert et al. 2002; Kienast et al. 2005; Grosse et al. 2007). A gradual transition to shallow fluvial deposition at the study site is indicated by the occurrence of grass roots in the uppermost horizon of unit A (>44.5 Kya). During the final stage of deposition of unit A, the initial composite sand–ice wedge formation coincided with the termination of fluvial activity. As these composite wedges are well preserved, we conclude that the river was only episodically active, with shallow water conditions by that time, and thereafter.

The shallow water conditions continued to about 45–40 Kya during the Kargin interstadial period. The entire length of the more moderate Kargin period in

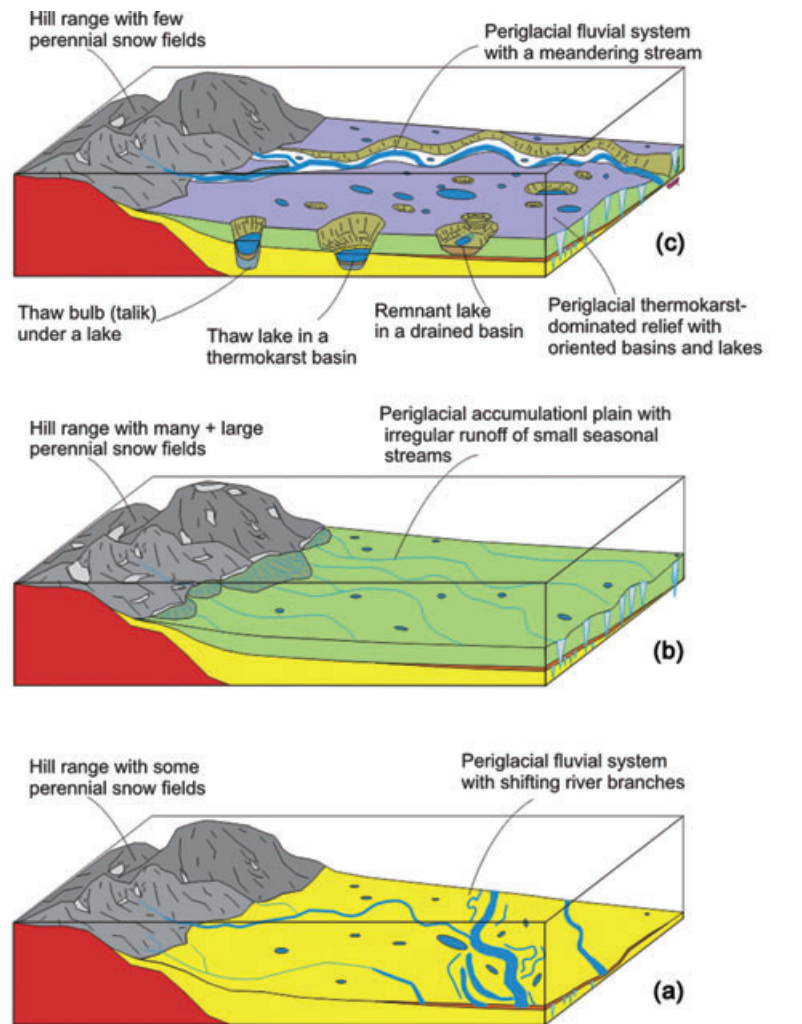


Fig. 11 Scheme of the Late Quaternary landscape dynamics. (a) High-energetic fluvial runoff and river flood plain sedimentation along the Pronchishchev Ridge during the Zyryan and Kargin period. (b) Low-energetic seasonal slope wash runoff over a flat accumulation plain connected with Ice Complex formation during the Sartan period. (c) Permafrost degradation (thermokarst and thermoerosion), beginning with the Late Pleistocene–Holocene transition period, and establishment of the modern hydrological regime.

Siberia corresponds to the Middle Weichselian interstadial or MIS 3. The following peat–sand alternation of unit B was probably formed by variable accumulation conditions on a floodplain terrace or in silted-up oxbow lakes. The peat–sand complex of unit B is composed of four peat beds with high TOC contents, alternating with sandy interbeds with very low TOC contents. It thus demonstrates a highly variable environment. The high C/N ratios accompanying the high TOC contents are an indi-

cation of limited decomposition of organic matter under anaerobic conditions, such as those found in swampy and waterlogged areas. They also indicate quick freezing and transformation into permafrost deposits. The flooding of the area that led to the deposition of sand occurred in alternation with the stagnant water periods that are favourable for plant growth and the accumulation of organic material. The formation of a generation of smaller ice wedges connected with separate peat layers proves the

existence of ice-wedge polygons, which were repeatedly buried by peat and sand. Finally, the sequence is the first evidence of well-dated Kargin deposits that do not belong to Ice Complex sequences, as is usually the case in the Laptev Sea region.

The fluvial phase terminated with the accumulation of the Ice Complex (unit C). According to pollen data, the Ice Complex formation had already begun at the end of the Kargin interstadial, and continued during the Sartan stage (corresponding to the Late Weichselian glaciation, MIS 2). Surface conditions that remained stable over long periods with extremely cold winters permitted the formation of extensive ice-wedge polygons on the flat accumulation plain in front of the Pronchishchev Ridge (Figs. 1, 11b). Perhaps the palaeoriver channel that deposited units A and B was affected by drastically falling discharge as a result of decreasing precipitation during the late Weichselian, when the climate was most continental. The accumulation of the fine-grained silty sand occurred within polygon centres. The slow transport and the rapid embedding of sediments into the permafrost favoured the deposition and preservation of organic remains usable as environmental indicators. Pollen, plant macro remains and mammal bones indicate the existence of a mammoth steppe environment under a cold and dry continental climate. Ice wedges developed syngenetically with continuous sedimentation during the entire Sartan stage. The transition of unit B to the Ice Complex is characterized by an increase in the silt fraction, pointing to a generally low level of transport energy in the hydrological system.

Because of the poorly sorted silt and sand fractions, we conclude that the Ice Complex deposits of unit C are not primarily of aeolian origin. This may contradict the current concept of "Arctic loess" (e.g., Tomirdiario 1982). For the deposits studied, we assume initial niveo-aeolian accumulation of clastic material in snow patches and névés in the nearby Pronchishchev Ridge, in accordance with Kunitsky et al. (2002). These sediments were subsequently redistributed by irregular meltwater run-off onto the accumulation plain. Along the transport path additional frost weathering products were included, and the poorly sorted sediments finally accumulated in the low centre polygons. This combination of processes would explain both the aeolian grain fraction and the low sorting of the studied Ice Complex deposits.

The general accumulation pattern did not change during the Sartan period. Relatively constant medium TOC contents are an indication of stable plant growth and more or less uniform surface conditions. C/N ratios lower than those in the peat horizons of unit B point to relatively dry and rather aerobic conditions in the active layer, with enhanced decomposition of the organic material. Based on the decrease in grain size accompanying the

formation of this unit, a floodplain with no permanent direct fluvial influence can be assumed as the accumulation environment. The run-off as main sediment supply was characterized by very low flow velocities, with little discharge in general and without a dominant direction. Irregular slope run-off originating in the Pronchishchev Ridge probably replaced the river flood plain facies during that period.

According to heavy mineral analysis, the source area of sediments did not change during the entire Late Pleistocene time span. This implies only hydrological reorganization of the local catchment area and no large-scale changes, as has been concluded for the Lena Delta region (Schwamborn et al. 2002; Schirrmeister et al. 2003).

The geological structure of the section studied implies that the modern coast cuts into a former depression in the sandy and peaty-sandy deposits of units A and B, which was later filled by Ice Complex deposits in the Late Pleistocene (unit C). After filling the depression, the Ice Complex sediments subsequently covered the whole area.

The general lateral architecture of the coastal section of Cape Mamontov Klyk (Fig. 2), i.e., the elevation and age relationships between the units A–C, lead us to conclude that the region subsided locally during the Late Weichselian Ice Complex accumulation. Between sandy sequences that accumulated until about 40–45 Kya, and exposed to a height of 10–15 m a.s.l., the coastal section contains younger deposits of the continuous Ice Complex sequence (Fig. 2). These are exposed laterally between the sandy units at sea level along a distance of several kilometres, and they also cover the sandy deposits along the coast. The two geochronologically well-correlated Ice Complex sequences indicate simultaneous sedimentation of ice-rich permafrost deposits at different elevation levels (Fig. 7). We here speculate that neotectonic subsidence of a local graben structure was compensated by Ice Complex deposition during the Sartan period.

The occurrence of deposits correlated with the Allerød interstadial in the lower part of unit D₁, below the bottom of a thermoerosional valley and a hiatus between late glacial and early Holocene deposits, verifies the beginning of permafrost degradation resulting from climate warming already starting at the end of the Late Pleistocene. The presence of sub-Arctic shrub-tundra with dominating *A. fruticosa* and *Betula* sect. *Nanae*, as evidenced by pollen and plant macro remains, indicates warm conditions with a mean temperature in the warmest month up to 10°C. Thermal degradation of the Ice Complex is indicated by wetland plants in pollen and macrofossil records. The sedimentation on top of the Ice Complex (unit D₂) started locally during the early Holocene, when small initial thermokarst depressions were formed. There is a gap in

the geochronological sequence of about 6 Ky, between 9.5 and 2.7 Kya, that was probably caused by thermoerosion. The phenomenon of local early Holocene sedimentation in small thermokarst depressions on top of the Ice Complex is reported in several studies around the Laptev Sea (Schirrmeister et al. 2002; Andreev et al., in press; Wetterich et al. 2008). Ice Complex degradation during the onset of Holocene warming caused the formation of the numerous thermokarst depressions that are widely distributed on the accumulation plain (Fig. 11c). About three-quarters of the modern coastal plain in the study area is affected by thermokarst and thermoerosional processes (Grosse et al. 2007), which is characteristic for lowland areas in north-east Siberia. Because of age reversals, the thermokarst depression sequences allow only a general palaeoenvironmental interpretation. The youngest ages might indicate the time of lake drainage by coastal erosion.

Conclusions

The coastal exposures of Mamontov Klyk in the western Laptev Sea represent four environmental stages of the northern plain of the Pronchishchev Ridge. This periglacial plain evolved under changing hydrological regimes that were most likely related to broader environmental changes. Initially, a fluvial run-off system (possibly south-east/north-west oriented) existed along the north side of the Pronchishchev Ridge. This fluvial system gradually shifted to an irregular slope run-off system (south-west/north-east oriented), originating in the hills and discharging over a wide floodplain with highly seasonal and overall low discharge rates. Both regimes resulted in the accumulation of permafrost deposits during the Early to Late Weichselian.

A further dramatic reorganization of the landscape was connected with degradation of these ice-rich permafrost sequences by thermokarst and thermoerosional processes during the warmer and moister Allerød and the early Holocene. The existing run-off system of the accumulation plain was reorganized towards numerous local catchments, with individual thermokarst depressions and lakes. Continuing postglacial sea-level rises during the Holocene lifted the erosional basis of the modern run-off system. This shifting hydrological regime, which appears to be typical across the north-east Siberian lowlands during the Late Pleistocene, is similar in its dimension and environmental effects to the rerouting of the northern Eurasian drainage during the Early to Late Weichselian, as reported by Mangerud et al. (2004).

The reconstructed Late Quaternary climate and environmental dynamics in the western Laptev Sea are comparable with similar reconstructions in regions

further east. This especially applies to the large fluvial run-off along the mountain chains from 100 to about 40 Kya (Siegert et al. 2002; Wetterich et al. 2008). The exposures indicate alluvial conditions with sandy peat accumulation on the shelf plain for the Kargin interstadial period. Further to the eastern Laptev Sea region, this period is frequently characterized by Ice Complex sequences only (e.g., Schirrmeister, Siegert, Kunitsky et al. 2002; Schirrmeister, Siegert, Kuznetsova et al. 2002; Andreev et al., in press). The typically open tundra-steppe vegetation attests to a relatively moderate and humid interstadial climate. The LGM period (Sartan glaciation) was characterized by continuous accumulation of ice-rich permafrost deposits between 27 and 15 Kya under very cold and dry climate conditions. Here we present the only continuous Sartan record in the Laptev Sea region besides the sequence on Bykovsky Peninsula, south-east of the Lena Delta (Andreev et al. 2002; Kienast et al. 2005).

Palaeoecological results, as well as $\delta^{13}\text{C}$ data from organic matter, indicate that only freshwater aquatic and subaerial terrestrial environments without connections to marine or brackish environments, as mentioned by Bol'shijanov et al. (2007), existed on the accumulation plain in front of the Pronchishchev Ridge as a part of the exposed Laptev shelf between about 50 Kya and today. The Mamontov Klyk sedimentary record is one of the westernmost Late Quaternary archives of the non-glaciated Beringian landmass. It closes a gap between the Taymyr Peninsula and the Lena River Delta in the nevertheless still wide-meshed net of palaeoclimate datasets for the Quaternary environment of the Eurasian north. The periglacial dynamics of our study area in the western Laptev shelf lowlands were likely to have been connected with Late Pleistocene dynamics of the Eurasian ice caps, located on the Putorana Plateau (about 900 km south-west of the study area) and on the north coast of the Taymyr Peninsula (about 500 km north-west of the study area), at about 90 and 60 Kya (Svendsen et al. 2004). During that time the Khatanga and Anabar rivers drained parts of the glacial meltwater towards the western Laptev shelf (Kleiber et al. 2001). Although the fluvial activity in our study area is of periglacial and not of glacial origin, there is a clear signal of high fluvial activity in the region during that period. During the LGM, the Eurasian ice sheet was smaller in extent than in the previous stadials, with a probably ice-free Putorana Plateau, and a limited glaciation on the Taymyr Peninsula. During the same period, the deposition patterns in our study region changed from sandy sediments towards the accumulation of the fine-grained ice-rich sediments of the Ice Complex indicative of a highly continental climate and a strongly seasonal hydrological regime.

Acknowledgements

The German Federal Ministry of Education and Research supported this study within the framework of the BMBF project 03G0859 (Process Studies of Permafrost Dynamics in the Laptev Sea). In addition, the German Research Foundation funded this study through the DFG projects SCHI 975/1 (Late Quaternary Warm Phases in the Arctic) and KI 849/1 (Environmental History of Northern Siberia), and the Russian–German co-operation was financially supported by German Research Foundation guest science support.

References

- Aitken M.J. 1998. *An introduction to optical dating*. Oxford: Oxford University Press.
- Andreev A., Grosse G., Schirrmeister L., Kuznetsova T.V., Kuzmina S.A., Bobrov A.A., Tarasov P.E., Novenko E.Y., Meyer H., Derevyagin A.Y., Kienast F., Bryantseva A. & Kunitsky V.V. in press. Weichselian and Holocene palaeo-environmental history of the Bol'shoy Lyakhovsky Island, New Siberian Archipelago, Arctic Siberia. *Boreas*.
- Andreev A.A., Schirrmeister L., Siebert C., Bobrov A.A., Demske D., Seiffert M. & Hubberten H.-W. 2002. Paleoenvironmental changes in north-eastern Siberia during the Late Pleistocene—evidence from pollen records of the Bykovsky Peninsula. *Polarforschung* 70, 13–25.
- Berglund B.E. & Ralska-Jasiewiczowa M. 1986. Pollen analysis and pollen diagrams. In B. Berglund (ed.): *Handbook of Holocene palaeo-ecology and palaeo-hydrology*. Pp. 455–484. New York: Interscience.
- Bojarskij O.G. & Mitt K.L. 1961. Novye dannye ob iskopaemykh l'dah v tundre Anabaro-Olenëkskogo meždurečija. (New data on relic ground ice in the tundra of the Anabar–Olenëk interfluvium.) *Merzlotnye Issledovanija* 1, 154–162. MSU Publishers.
- Bolshiyakov D. & Makarov A. 2004. Geomorphological route along the Urasalakh River. *Berichte zur Polar- und Meeresforschung* 489, 67–74.
- Bol'shijakov [Bolshiyakov] D.Ju., Grigoriev M.N., Schneider W., Rachold V., Overduin P., Hubberten H., Makarov A.S. & Gusev E.A. 2007. Kolebanija urovnja morej i formirovanie ledovogo kompleksa porod na poberež'e morej Laptevyyh v pozdnem neopleistotsene. (Sea level changes and the formation of glacial deposits in the coastal zone of the Laptev Sea during the Late Neopleistocene.) In: *Fundamental'nye problemy kvartera: itogi izučeniya i osnovnye napravlenija dal'neiših issledovanii*. (Fundamental problems of the Quaternary: results of investigations and main directions for further studies.) Pp. 45–49. Moscow: GEOS.
- Čekanovskiy N.L. 1896. *Dnevnik ekspedicii po rekam Nižnej Tunguske, Olenëku i Lene v 1873–1875 g.g.* (Fieldbook of the expeditions at the rivers Nižnjaja Tunguska, Olenëk and Lena in 1873–1875.) *Zapiski Russkogo Geografičeskogo obščestva* 20 (1). (Transactions of the Russian Geographical Society 20 [1]). St. Petersburg.
- Dierßen K. 1996. *Vegetation Nordeuropas*. (The vegetation of northern Europe.) Stuttgart: Eugen Ulmer Verlag.
- Drachev S.S., Savostin L.A., Groshev V.G. & Bruni I.E. 1998. Structure and geology of the continental shelf of the Laptev Sea, eastern Russia Arctic. *Tectonophysics* 298, 357–393.
- Grosse G., Schirrmeister L. & Malthus T.J. 2006. Application of Landsat-7 satellite data and a DEM for the quantification of thermokarst-affected terrain types in the periglacial Lena–Anabar coastal lowland. *Polar Research* 25, 51–67.
- Grosse G., Schirrmeister L., Siebert C., Kunitsky V., Slagoda E.A., Andreev A.A. & Dereviagin A.Y. 2007. Geological and geomorphological evolution of a sedimentary periglacial landscape in northeast Siberia during the Late Quaternary. *Geomorphology* 86, 25–51.
- Kienast F., Schirrmeister L., Siebert C. & Tarasov P. 2005. Palaeo-botanical evidence for warm summers in the east Siberian Arctic during the last cold stage. *Quaternary Research* 63, 283–300.
- Kienast F., Tarasov P., Schirrmeister L., Grosse G. & Andreev A.A. 2008. Continental climate in the east Siberian Arctic during the last interglacial: implications from palaeobotanical records. *Global and Planetary Change* 60, 535–562.
- Kleiber H.P., Niessen F., Weiel D. 2001. The Late Quaternary evolution of the western Laptev Sea continental margin, Arctic Siberia—implications from sub-bottom profiling. *Global and Planetary Change* 31, 105–124.
- Kolpakov V.V. 1973. Paleogeografičeskoe značenie četvertičnyh eolovyh otloženii severa vostočnoj Sibiri. (The paleogeographical significance of Quaternary aeolian deposits in the north of eastern Siberia.) In: *Nekotorye voprosy regionalnoj geologii*. (Some problems of regional geology.) Pp. 38–42. Moscow: Moscow University Publishing.
- Kulig G. 2005. *Erstellung einer Auswertesoftware zur Altersbestimmung mittels Lumineszenzverfahren unter spezieller Berücksichtigung des Einflusses radioaktiver Ungleichgewichte in der 238U-Zerfallsreihe*. (Programming of an analysis software for age determination using luminescence methods taking into account influences of radioactive disequilibria of the 238U decay series.) BSc thesis, Dept. of Geology, Technische Universität Bergakademie Freiberg, Germany.
- Kunitsky V.V., Schirrmeister L., Grosse G. & Kienast F. 2002. Snow patches in nival landscapes and their role for the Ice Complex formation in the Laptev Sea lowlands. *Polarforschung* 70, 53–67.
- Kuznetsova T.V. 2004. Paleontological studies. In L. Schirrmeister et al. (eds.): *Russian–German cooperation System Laptev Sea: the Expedition Lena–Anabar 2003*. *Berichte zur Polar- und Meeresforschung* 489, 135–138, 189–209.
- Malyshev L.I. & Peschkova G.A. 2003. *Portulacaceae–Ranunculaceae. Flora of Siberia* 6. Enfield, NH: Science Publishers.

- Mangerud J.M., Jacobsson M., Alexanderson H., Astakhov V., Clarke G.K.C., Henriksen M., Hjort C., Krinner G., Lunkka J.-P., Möller P., Murray A., Nikolskaya O., Saarnisto M. & Svendsen J.I. 2004. Ice-dammed lakes and rerouting of the drainage of northern Eurasia during the last glaciation. *Quaternary Science Reviews* 23, 1313–1332.
- Meyer H., Dereviagin A.Y., Siegert C. & Hubberten H.-W. 2002. Paleoclimate studies on Bykovsky Peninsula, north Siberia—hydrogen and oxygen isotopes in ground ice. *Polarforschung* 70, 37–51.
- Meyer H., Dereviagin A.Y., Siegert C., Schirrmeyer L. & Hubberten H.-W. 2002. Paleoclimate reconstruction on Big Lyakhovsky Island, north Siberia—hydrogen and oxygen isotopes in ice wedges. *Permafrost and Periglacial Processes* 13, 91–105.
- Möller I. 2000. *Studien zur Vegetation Nordwestspitzbergens. (Studies of the vegetation in north-west Spitsbergen.)* PhD thesis, Dept. of Geoscience, University of Hamburg.
- Murray A.S., Svendsen J.I., Mangerud J. & Astakhov V.I. 2007. Testing the accuracy of quartz OSL dating using a known-age Eemian site on the river Sula, northern Russia. *Quaternary Geochronology* 2, 102–109.
- Murray A.S. & Wintle A.G. 2000. Luminescence dating of quartz using an improved single-aliquot regenerative-dose protocol. *Radiation Measurements* 33, 57–73.
- Nadeau M.J., Grootes P.M., Schleicher M., Hasselberg P., Rieck A. & Bitterling M. 1998. Sample throughput and data quality at the Leibniz-Labor AMS facility. *Radiocarbon* 40, 239–245.
- Nadeau M.J., Schleicher M., Grootes P.M., Erlenkeuser H., Gott dang A., Mous D.J.W., Sarntheim J.M. & Willkomm H. 1997. The Leibniz-Labor facility at the Christian-Albrecht-University, Kiel, Germany. *Nuclear Instruments and Methods in Physics Research* 123, 22–30.
- Overduin P.P., Grigoriev M.N., Junker R., Rachold V., Kunitsky V.V., Bolshiyarov D.Y. & Schirrmeyer L. 2007. The Expedition COAST I: COAST drilling campaign 2005: subsea permafrost studies in the near-shore zone of the Laptev Sea. *Berichte zur Polar- und Meeresforschung* 550, 1–40.
- Prescott J.R. & Hutton J.T. 1994. Cosmic ray contribution to dose rates for luminescence and ESR dating: large depth and long term time variations. *Radiation Measurements* 23, 497–500.
- Preusser F., Blei A., Graf H.R. & Schlüchter C. 2007. Luminescence dating of Würmian (Weichselian) proglacial sediments from Switzerland: methodological aspects and stratigraphical conclusions. *Boreas* 36, 130–142.
- Preusser F. & Kasper H.U. 2001. Comparison of dose rate determination using high-resolution gamma spectrometry and inductively coupled plasma–mass spectrometry. *Ancient TL* 19, 17–21.
- Puminov A.P. 1962. Pokrovyne obrazovanija Anabaro-Olenëkskogo meždurečija. (Quaternary cover sediments of the Anabar-Olenëk interfluve.) *Trudy Instituta Geologii i Geofiziki* 27, 102–117.
- Rachold V., Bolshiyarov Y., Grigoriev M.N., Hubberten H.-W., Junker R., Kunitsky V.V., Merker F., Overduin P.P. & Schneider W. 2007. Nearshore Arctic subsea permafrost in transition. *EOS, Transactions of the American Geophysical Union* 88, 149–156.
- Saks V.N. 1953. *Četvertičnyj period v Sovetskoj Arktike. (Quaternary period in the Soviet Arctic.)* *Trudy Naučno-issledovatel'skogo Instituta Geologii Arktiki (NIIGA)* 77. Leningrad: Institute of Arctic Geology.
- Schirrmeyer L., Grigoriev M.N., Kutzbach L., Wagner D. & Bolshiyarov D.Y. (eds.) 2004. Russian–German cooperation System Laptev Sea: the Expedition Lena–Anabar 2003. In L. Schirrmeyer (ed.): *Expeditions to Siberia 2003. Berichte zur Polar- und Meeresforschung* 489.
- Schirrmeyer L., Grosse G., Schwamborn G., Andreev A.A., Meyer H., Kunitsky V.V., Kuznetsova T.V., Dorozhkina M.V., Pavlova E. Y., Bobrov A.A. & Oezen D. 2003. Late Quaternary history of the accumulation plain north of the Chekanovsky Ridge (Lena Delta, Russia): a multidisciplinary approach. *Polar Geography* 27, 277–319.
- Schirrmeyer L., Meyer H., Wetterich S., Siegert C., Kunitsky V.V., Grosse G., Kuznetsova T.V. & Dereviagin A.Ju. 2008. The Yedoma suite of the northeastern Siberian shelf region: characteristics and concept of formation. In D.L. Kane & K.M. Hinkel (eds.): *Ninth International Conference on Permafrost*. Pp. 1595–1600. Fairbanks, AK: Institute of Northern Engineering, University of Alaska Fairbanks.
- Schirrmeyer L., Siegert C., Kunitsky V.V., Grootes P.M. & Erlenkeuser H. 2002. Late Quaternary ice-rich permafrost sequences as a paleoenvironmental archive for the Laptev Sea region in northern Siberia. *International Journal of Earth Sciences* 91, 154–167.
- Schirrmeyer L., Siegert C., Kuznetsova T., Kuzmina S., Andreev A.A., Kienast F., Meyer H. & Bobrov A.A. 2002. Paleoenvironmental and paleoclimatic records from Permafrost deposits in the Arctic region of Northern Siberia. *Quaternary International* 89, 97–118.
- Schwamborn G., Rachold V. & Grigoriev M.N. 2002. Late Quaternary sedimentation history of the Lena Delta. *Quaternary International* 89, 119–134.
- Siegert C., Schirrmeyer L. & Babiy O. 2002. The sedimentological, mineralogical and geochemical composition of late Pleistocene deposits from the ice complex on the Bykovsky Peninsula, northern Siberia. *Polarforschung* 70, 3–11.
- Sočava V.B. 1933. *Tundra bassejna reki Anabar. (The tundra of the Anabar River basin.)* *Izvestija Gosudarstvennogo Geografičeskogo obščestva* 65.
- Solov'ev P.A. 1959. *Kriolitozona severnoj časti Leno-Amginskogo meždurečija. (The cryolith zone in the northern part of the Lena–Amga interfluve.)* Moscow: Publications of the Academy of Science of the USSR.
- Solov'ev P.A. 1989. Karta mnogoletnej merzloty (kriolitozony) Jakutskoj ASSR Masštab 1 : 10 000 000. (Permafrost [cryolith zone] map of Yakutia, scale 1 : 10 000 000.) In I.A. Matveev et al. (eds.): *Atlas sel'skogo*

- hozjajstva Jakutskoj ASSSR. (*Agricultural atlas of the Yakutian ASSR*.) P. 27. Moscow: Moscow GUGK Publishers.
- Svendsen J.I., Alexanderson H., Astakhov V.I., Demidov I., Dowdeswell J.A., Funder S., Gataullin V., Henriksen M., Hjort C., Houmark-Nielsen M., Hubberten H.-W., Ingólfsson O., Jacobsson M., Kjaer K., Larsen E., Lokrantz H., Lunkka J.P., Lyså A., Mangerud J., Matioushkov A., Murray A., Möller P., Niessen F., Nikolskaya O., Polyak L., Saarnisto M., Siegert C., Siegert M.J., Spielhagen R.F. & Stein R. 2004. Late Quaternary ice sheet history of northern Eurasia. *Quaternary Science Reviews* 23, 1229–1272.
- Toll E.V. 1894. *Ekspeditsija Imperatorskoj Akademii Nauk 1893 g. na Novosiborskie Ostrova i poberež'e Ledovitogo Okeana. (The expedition of the Imperial Academy of Science to the New Siberian Islands and coast of the Arctic Ocean.) Izvestija Russkogo Geografičeskogo obščestva* 30.
- Tolmačev I.P. 1905. *O novyh nahodkah po geologii Sibirii. (New findings about Siberia's geology.) Trudy Peterburgskogo obščestva estestvoispytatelej* 24.
- Tolmachev A.I. 1995. *Flora of the Russian Arctic. Vol. 1. Polypodiaceae–Gramineae.* J.G.W. Packer (ed.), G. Griffiths (trans.). Edmonton: University of Alberta Press.
- Tolmachev A.I. 1996. *Flora of the Russian Arctic. Vol. 1. Cyperaceae–Orchidaceae.* J.G.W. Packer (ed.), G. Griffiths (trans.). Edmonton: University of Alberta Press.
- Tolmachev A.I. 2000. *Flora of the Russian Arctic. Vol. 3. Salicaceae–Ranunculaceae.* J.G.W. Packer (ed.), G. Griffiths (trans.). Stuttgart: J. Cramer.
- Tomirdiaro S.V. 1982. Evolution of lowland landscapes in northern Asia during Late Quaternary time. In D.V. Hopkins et al. (eds.): *Paleoecology of Beringia*. Pp. 29–37. New York: Academic Press.
- UNEP/GRID-Arendal 2005. *Permafrost distribution in the Arctic.* P. Rekacewicz (cartographer/designer). UNEP/GRID-Arendal Maps and Graphics Library. Accessed on the internet at <http://maps.grida.no/go/graphic/permafrost-distribution-in-the-arctic> on 17 May 2008.
- van Everdingen R.O. (ed.) 1998. *Multi-language glossary of permafrost and related ground-ice terms.* Calgary: Arctic Institute of North America, University of Calgary.
- Weber H.E., Moravec J., Theurillat J.-P. 2000. International code of phytosociological nomenclature. 3rd edition. *Journal of Vegetation Sciences* 11, 739–768.
- Wetterich S., Kuzmina S., Kuznetsova T., Andreev A.A., Kienast F., Meyer H., Schirrmeister L. & Sierralta M. 2008. Palaeoenvironmental dynamics inferred from late Quaternary permafrost deposits on Kurungnakh Island, Lena Delta, northeast Siberia, Russia. *Quaternary Science Reviews*, doi:10.1016/j.quascirev.2008.04.007
- Williams P.J. & Warren I.M.T. 1999. *Geocryological map of Russia and neighbouring republics, 1 : 2,500,000 scale. The English-language edition.* Ottawa: Geotechnical Science Laboratories, Carleton University.
- Wintle A.G. & Murray A.S. 2006. A review of quartz optically stimulated luminescence characteristics and their relevance in single-aliquot regeneration dating protocols. *Radiation Measurements* 41, 369–391.
- Žukov V.V., Gorina I.F. & Pinčuk L.Ja. 1968. *Kainozoiskie almazonosnye rossypi Anabaro-Oleněkskogo međdurečija (uslovija formirovanija i zakonomernosti razmešenija). [Cenozoic diamondiferous placer deposits of the Anabar–Olenëk interfluve (conditions of formation and regularity of distribution)].* Moscow: Nedra Publishers.